

CLEARED
FOR PUBLIC RELEASE

PLIPA 5/15/97

Sensor and Simulation Notes

Note 120

October 1970

Low-Frequency Magnetic Field Interaction of a Half Toroid
Simulator With a Perfectly Conducting Hemisphere

A. D. Varvatsis and M. I. Sancer
Northrop Corporate Laboratories
Pasadena, California

Abstract

In this note we consider the situation where the half toroid is joined to a perfectly conducting half space upon which the hemisphere rests. The half toroid is modeled as an infinitely thin semi-circular current loop. We settle some subtle questions concerning the method of images and derive three suitable image currents to solve for the magnetic field on the surface of the hemisphere. This field is compared to the field which would exist in the limit $a/b \rightarrow \infty$ where a is the radius of the half toroid and b is the radius of the hemisphere. In this limit the half toroid tends to simulate the low frequency magnetic field corresponding to the electromagnetic pulse. Plots are given which indicate the simulation trade off one must accept with a finite a/b .

PL 96-1175

I. Introduction

In this note we consider the interaction of the half toroid simulator with a perfectly conducting hemisphere situated on the ground. The geometry of the simulator has been described in a previous note¹. The center of the hemisphere coincides with the origin of our coordinate system as depicted in figure 1. In this figure the toroid is depicted as a half loop. The justification for this is that the major radius of the toroid is assumed to be much larger than its minor radius. We are interested in the low frequency interaction and consequently we assume that in this limit the simulator can be represented by a constant current flowing in this half loop. We assume the ground to be infinitely conducting in order to facilitate the analysis. The conditions under which the finitely conducting ground can be considered perfectly conducting are presently being studied. In summary, the problem we will solve is that of the magnetostatic interaction of a constant current half loop joined to a perfectly conducting half space with a perfectly conducting hemisphere resting upon the half space. In particular we will solve for the magnetic field on the surface of the hemisphere.

We perform this calculation in order to determine how the finite size of the toroid limits its function as a simulator. We solve for the magnetic field at any point on the surface of the hemisphere as a function of the toroid's inclination angle ξ_1 and the ratio of the toroid's radius to the radius of the hemisphere, a/b . As a/b approaches infinity the toroid tends to simulate the low frequency limit of the magnetic field corresponding to the electromagnetic pulse. One of our tasks is to determine the value of a/b that allows us to come sufficiently close to the value of the limit within a specified engineering accuracy. An important quantity which can be used to decide the engineering value of a/b is the magnetic field deviation D_v . This quantity is defined as the magnitude of the vector difference of the actual total magnetic field and the limiting total magnetic field. The maximum, D_v , occurs at the intersection of the plane of the loop, the surface of the hemisphere, and the x - z plane which is the symmetry plane of the half loop. For a fixed ξ_1 and a/b the value of D_v does not appreciably deviate from the maximum D_v along most of the intersection of the plane of the loop and the surface of the hemisphere. For an inclination angle different from zero, the

value of D_V along this intersection changes appreciably only near the point where the loop joins the ground. This change is most pronounced for large inclination angles. The value of D_V does change significantly as we move perpendicular away from the intersection curve.

The two other quantities which we study in this note are the spherical components of the total magnetic field on the surface of the hemisphere. We normalize these components with respect to the magnitude of the total surface magnetic field which corresponds to the limit as a/b approaches infinity. These quantities are plotted versus a/b with ξ_1 and the spherical angles θ and ϕ as parameters. These plots show how the distribution of the field on the hemisphere is affected by ξ_1 and the ratio a/b .

Our method of solution is based on the method of images. The use of this method in electrostatics is straightforward; however, its application in magnetostatics involves subtle points. To attack this problem we considered a current element and studied its properties. A current element has a non-zero divergence and does not satisfy the usual magnetostatic equation. To handle this difficulty we modeled the current element in such a way that the fields associated with it satisfy the time-dependent Maxwell's equation. It was found that given the proper interpretation one can use the method of images for a constant current element that has non-zero divergence. The details concerning this point are presented in the appendix. Based on this result we were able to apply the method of images to our problem.

II. Formulation

Using the method of images the magnetic field at any point is the sum of the magnetic fields caused by four semicircular current loops oriented as in figure 2. The four semicircular current loops are derived as follows. First we consider the mirror images of the original half loop and the hemisphere with respect to the ground plane. The current of the image half loop is equal to the current I of the original half loop and it flows in a way that preserves current continuity. At this stage we have reduced our problem to that of the interaction of a perfectly conducting sphere and a symmetrically bent loop of radius a . Next we substitute the sphere by two image half loops that constitute a symmetrically bent loop carrying a current $(a/b)I$ and having a radius b^2/a where b is the radius of the sphere. The flow of the current in this latter loop is opposite to the flow of the current I . In figure 3 we define a Cartesian coordinate system so that a typical current loop lies in the $u_1^i - u_2^i$ plane and the corresponding cylindrical coordinates $(\lambda^i, \beta^i, u_3^i)$ are also used. The superscript i ranges from 1 to 4 corresponding to each of the four loops. The calculation of the magnetic field due to a particular loop in its own coordinate system has been performed in a previous note². The results for the normalized magnetic field, $\underline{h} = (2a/I)\underline{H}$, are

$$h_{\lambda}^i = \frac{1}{8\pi} \frac{B_i}{A_i} \left(\frac{m_i}{A_i}\right)^{\frac{1}{2}} \left\{ \frac{2-m_i}{m_{1i}} \left[E\left(\frac{\pi+\beta_i}{2} \middle| m_i\right) - E\left(\frac{\beta_i}{2} \middle| m_i\right) \right] - 2 \left[F\left(\frac{\pi+\beta_i}{2} \middle| m_i\right) - F\left(\frac{\beta_i}{2} \middle| m_i\right) \right] \right. \\ \left. + \frac{m_i}{m_{1i}} (2-m_i) \sin \frac{\beta_i}{2} \cos \frac{\beta_i}{2} \left\{ \left[1-m_i \sin^2\left(\frac{\beta_i}{2}\right) \right]^{-\frac{1}{2}} + \left[1-m_i \cos^2\left(\frac{\beta_i}{2}\right) \right]^{-\frac{1}{2}} \right\} \right\} \quad (1)$$

$$h_{\beta}^i = \frac{1}{4\pi} \frac{B_i}{A_i} \left(\frac{m_i}{A_i}\right)^{\frac{1}{2}} \left\{ - \left[1-m_i \sin^2\left(\frac{\beta_i}{2}\right) \right]^{-\frac{1}{2}} + \left[1-m_i \cos^2\left(\frac{\beta_i}{2}\right) \right]^{-\frac{1}{2}} \right\} \quad (2)$$

$$h_3^i = \frac{1}{2\pi} A_i^{-3/2} m_i^{\frac{1}{2}} \left\{ \frac{1}{4m_{1i}} \left[(1+A_i)m_i - 2A_i \right] \left[E\left(\frac{\pi+\beta_i}{2} \middle| m_i\right) - E\left(\frac{\beta_i}{2} \middle| m_i\right) \right] + \frac{A_i}{2} \left[F\left(\frac{\pi+\beta_i}{2} \middle| m_i\right) - F\left(\frac{\beta_i}{2} \middle| m_i\right) \right] \right. \\ \left. + \frac{m_i}{4m_{1i}} \left[(1+A_i)m_i - 2A_i \right] \sin \frac{\beta_i}{2} \cos \frac{\beta_i}{2} \left\{ \left[1-m_i \sin^2\left(\frac{\beta_i}{2}\right) \right]^{-\frac{1}{2}} + \left[1-m_i \cos^2\left(\frac{\beta_i}{2}\right) \right]^{-\frac{1}{2}} \right\} \right\} \quad (3)$$

where

$$A_1 = \left(\frac{r}{a}\right) \left\{ (\sin \theta \cos \phi \cos \xi_1)^2 + (\sin \theta \sin \phi)^2 + (\cos \theta \sin \xi_1)^2 + \frac{1}{2} \sin 2\xi_1 \sin 2\theta \cos \phi \right\}^{\frac{1}{2}} \quad (4a)$$

$$A_2 = \left(\frac{a}{b}\right)^2 A_1 \quad (4b)$$

$$A_3 = \left(\frac{r}{a}\right) \left\{ (\sin \theta \cos \phi \cos \xi_1)^2 + (\sin \theta \sin \phi)^2 + (\cos \theta \sin \xi_1)^2 - \frac{1}{2} \sin 2\xi_1 \sin 2\theta \cos \phi \right\}^{\frac{1}{2}} \quad (5a)$$

$$A_4 = \left(\frac{a}{b}\right)^2 A_3 \quad (5b)$$

$$B_1 = \left(\frac{r}{a}\right) \{-\sin \xi_1 \sin \theta \cos \phi + \cos \xi_1 \cos \theta\} \quad (6a)$$

$$B_2 = \left(\frac{a}{b}\right)^2 B_1 \quad (6b)$$

$$B_3 = \left(\frac{r}{a}\right) \{\sin \xi_1 \sin \theta \cos \phi + \cos \xi_1 \cos \theta\} \quad (7a)$$

$$B_4 = \left(\frac{a}{b}\right)^2 B_3 \quad (7b)$$

$$\beta_1 = \beta_2 = \arctan \frac{\delta_1}{\gamma_1}$$

$$\delta_1 = \sin \theta \cos \phi \cos \xi_1 + \cos \theta \sin \xi_1$$

$$\gamma_1 = -\sin \theta \sin \phi \quad (8)$$

$$\beta_3 = \beta_4 = \arctan \frac{\delta_3}{\gamma_3}$$

$$\delta_3 = -\sin \theta \cos \phi \cos \xi_1 + \cos \theta \sin \xi_1$$

$$\gamma_3 = \sin \theta \sin \phi \quad (9)$$

$$m_1 = \frac{4A_1}{(1+A_1)^2 + B_1^2} = 1 - m_{11} \quad (10)$$

and $E(p|q)$ and $F(p|q)$ are elliptic integrals defined so that

$$E(p+s|q) - E(p|q) = \int_p^{p+s} (1 - q \sin^2 t)^{\frac{1}{2}} dt \quad (11)$$

$$F(p+s|q) - F(p|q) = \int_p^{p+s} (1 - q \sin^2 t)^{-\frac{1}{2}} dt \quad (12)$$

The signs of $\delta_1, \gamma_1, \delta_3$ and γ_3 determine the quadrant for the β 's as though they were polar angles in δ - γ planes. When comparing (1), (2) and (3) to the appropriate results in note 112 it is necessary to set $A_1 = \lambda/a$ and $B_1 = u_3/a$ where a is the radius of the semi-circular current loop. Before we can add the magnetic fields due to the four current loops we must change the normalized h 's to the actual field components through the relation $\underline{H} = (I/2a)\underline{h}$. I is the magnitude of the DC current flowing in the semi-circular loop. The current in the spherical image loop is $a/b I$ and this factor must be accounted for as well as the modified radius when adding the contribution of this loop. Taking these facts into account the procedure for adding the four loop contributions will now be given. We define

$$h_1^i = h_\lambda^i \cos \beta_i - h_\beta^i \sin \beta_i \quad i = 1, 2, 3, 4 \quad (13)$$

$$h_2^i = h_\lambda^i \sin \beta_i + h_\beta^i \cos \beta_i \quad i = 1, 2, 3, 4 \quad (14)$$

$$h_x^i = h_2^i \cos \xi_1 - h_3^i \sin \xi_1 \quad i = 1, 2 \quad (15)$$

$$h_y^i = -h_1^i \quad i = 1, 2 \quad (16)$$

$$h_z^i = h_2^i \sin \xi_1 + h_3^i \cos \xi_1 \quad i = 1, 2 \quad (17)$$

$$h_x^i = -h_2^i \cos \xi_1 + h_3^i \sin \xi_1 \quad i = 3, 4 \quad (18)$$

$$h_y^i = h_1^i \quad i = 3,4 \quad (19)$$

$$h_z^i = h_2^i \sin \xi_1 + h_3^i \cos \xi_1 \quad i = 3,4 \quad (20)$$

and add these quantities in a manner which accounts for the different radii, current strengths, and directions as follows:

$$h_x = h_x^1 - \left(\frac{a}{b}\right)^2 h_x^2 + h_x^3 - \left(\frac{a}{b}\right)^2 h_x^4 \quad (21)$$

$$h_y = h_y^1 - \left(\frac{a}{b}\right)^2 h_y^2 + h_y^3 - \left(\frac{a}{b}\right)^2 h_y^4 \quad (22)$$

$$h_z = h_z^1 - \left(\frac{a}{b}\right)^2 h_z^2 + h_z^3 - \left(\frac{a}{b}\right)^2 h_z^4 \quad (23)$$

We will present our results in spherical coordinates using the standard relationships

$$h_r = h_x \sin \theta \cos \phi + h_y \sin \theta \sin \phi + h_z \cos \theta \quad (24)$$

$$h_\theta = h_x \cos \theta \cos \phi + h_y \cos \theta \sin \phi - h_z \sin \theta \quad (25)$$

$$h_\phi = -h_x \sin \phi + h_y \cos \phi \quad (26)$$

In this note we restrict our observation point to lie on the surface of the hemisphere so that $r = b$ and h_r is calculated as a partial check of our program as it must equal zero.

Before we describe our main results it is necessary to present the limiting value of the magnetic field on the surface of the hemisphere as the ratio a/b tends to infinity. In the limit h has only a θ component which can be shown to be given by

$$h_{\theta L} = -\frac{3}{2} \sin \theta \cos \xi_1 \quad (27)$$

The quantities of interest are h_θ , h_ϕ , and $D_v = [(h_\theta - h_{\theta L})^2 + h_\phi^2]^{1/2}$. In graphically presenting our results we plot $|h_\theta/h_{\theta L}|$, $|h_\phi/h_{\theta L}|$, and $D = D_v/|h_{\theta L}|$

versus a/b with parameters θ , ϕ , and ξ_1 . The absolute magnitude symbol for $|h_\theta/h_{\theta L}|$ is superfluous since the h_θ and $h_{\theta L}$ always have the same sign; however, we will retain this symbol for the sake of uniformity. We also plot D corresponding to D_v maximized over the sphere. This D , referred to as D_m , is plotted versus a/b with only the inclination angle as a parameter. Specifically we plot $|h_\theta/h_{\theta L}|$, $|h_\phi/h_{\phi L}|$, and D versus a/b at points on the hemisphere for inclination angles $2\xi_1/\pi = 0, .2, .5, .7$ and $.9$. We also plot D_m versus a/b for these inclination angles. In particular for the quantities $|h_\theta/h_{\theta L}|$, $|h_\phi/h_{\phi L}|$, and D the spherical angles θ and ϕ also serve as parameters. We have selected $\theta = \pi/20, \pi/4, \pi/2, 3\pi/4$ and $19\pi/20$ and for each θ , ϕ assumes the values $0, \pi/6, \pi/3, \pi/2$. We have not considered the values $\theta = 0$ or π because all field components are zero irrespective of the value of ξ_1 or a/b . No negative values of ϕ are considered since our problem is symmetric with respect to the xz plane. The plots of $|h_\phi/h_{\phi L}|$ do not appear for ϕ equal to 0 or $\pi/2$ or $\xi_1 = 0$ because h_ϕ is zero for these cases.

The plots of $|h_\theta/h_{\theta L}|$, $|h_\phi/h_{\phi L}|$, and D show how at different points of the hemisphere and for different simulator inclination angles the relative size of the simulator, a/b , limits the behavior of the simulator. The D_m plot indicates a limitation which accounts for all observation angles on the hemisphere. Specifically the deviations of $|h_\theta/h_{\theta L}|$ from unity and $|h_\phi/h_{\phi L}|$, D , and D_m from zero indicate the simulation trade off one must accept with a finite a/b .

Table of Graphs

Figure Number	Quantity plotted versus a/b with ξ_1 as a parameter	θ coordinate of observation point on the hemisphere	ϕ coordinate of observation point on the hemisphere
6	$ h_\theta/h_{\theta L} $	$\pi/20$	0
7	—	—	$\pi/6$
8	—	—	$\pi/3$
9	—	—	$\pi/2$
10	—	$\pi/4$	0
11	—	—	$\pi/6$
12	—	—	$\pi/3$
13	—	—	$\pi/2$
14	—	$\pi/2$	0
15	—	—	$\pi/6$
16	—	—	$\pi/3$
17	—	—	$\pi/2$
18	—	$3\pi/4$	0
19	—	—	$\pi/6$
20	—	—	$\pi/3$
21	—	—	$\pi/2$
22	—	$19\pi/20$	0
23	—	—	$\pi/6$
24	—	—	$\pi/3$
25	—	—	$\pi/2$
26	$ h_\phi/h_{\theta L} $	$\pi/20$	$\pi/6$
27	—	—	$\pi/3$
28	—	$\pi/4$	$\pi/6$
29	—	—	$\pi/3$
30	—	$\pi/2$	$\pi/6$
31	—	—	$\pi/3$
32	—	$19\pi/20$	$\pi/6$
33	—	—	$\pi/3$
34	—	$3\pi/4$	$\pi/6$
35	—	—	$\pi/3$

Table of Graphs (continued)

Figure Number	Quantity plotted versus a/b with ξ_1 as a parameter	θ coordinate of observation point on the hemisphere	ϕ coordinate of observation point on the hemisphere
36	D	$\pi/20$	0
37	—	—	$\pi/6$
38	—	—	$\pi/3$
39	—	—	$\pi/2$
40	—	$\pi/4$	0
41	—	—	$\pi/6$
42	—	—	$\pi/3$
43	—	—	$\pi/2$
44	—	$\pi/2$	0
45	—	—	$\pi/6$
46	—	—	$\pi/3$
47	—	—	$\pi/2$
48	—	$3\pi/4$	0
49	—	—	$\pi/6$
50	—	—	$\pi/3$
51	—	—	$\pi/2$
52	—	$19\pi/20$	0
53	—	—	$\pi/6$
54	—	—	$\pi/3$
55	—	—	$\pi/2$
56	D_m	*	*
57	D_m	*	*

* No single observation point is associated with D_m because it results from a maximization procedure which allows θ and ϕ to range over the entire surface of the hemisphere.

III. Discussion of Numerical Results

All of the plots contained in figures 6 through 56 converge to the values one would expect. The observation points on the hemisphere corresponding to these plots are depicted in figure 5. When interpreting the data one might be concerned that the rate of convergence to the limiting values with increasing a/b is comparatively slow for observation points corresponding to θ equal to $\pi/20$ or $19\pi/20$. This is especially true for the plots of $|h_\theta/h_{\theta L}|$ and D versus a/b . When interpreting these plots one should be aware that $|h_\theta/h_{\theta L}|$ is relatively small for these observation angles, thus diminishing the significance of this comparatively slow convergence. The same discussion is also pertinent for the plots corresponding to $\theta = \pi/4$ and $3\pi/4$ as compared to the plots for $\theta = \pi/2$.

In figures 36, 40, 41, 43 and 44 certain plots contain sharp dips where the value of D drops to zero. These dips only occur when $h_\phi = 0$ and consequently $D = |1 - h_\theta/h_{\theta L}|$. As noted earlier $h_\theta/h_{\theta L}$ is always positive, but we retained the notion $|h_\theta/h_{\theta L}|$ when plotting this quantity for uniformity. By studying the corresponding smooth plots of this quantity in figures 6, 10, 11, 14 and 15 we see that $|h_\theta/h_{\theta L}|$ can equal one for finite values of a/b . We can understand how this is possible by considering figure 15. When the observation point is near the toroid then $|h_\theta/h_{\theta L}|$ is very large for small a/b while when the observation point is far from the toroid then $|h_\theta/h_{\theta L}|$ is small for small a/b . For large a/b , $|h_\theta/h_{\theta L}|$ approaches unity, independent of the observation point on the hemisphere. This explains the extreme curves corresponding to $2\xi_1/\pi$ equal to 0 and .9, the first being monotonically decreasing to unity while the second is monotonically increasing to unity. It is reasonable that an intermediate value, $2\xi_1/\pi = .2$, would correspond to a transition from a decreasing function to an increasing function which has a maximum that is greater than unity. It should be noted that the steepness of the dips is greatly exaggerated by the use of a logarithmic scale for the D plots.

Appendix

In electrostatics the method of images has gained considerable popularity mainly because of its simplicity. By choosing suitable image charges we can make the tangential component of the total electric field, along the surface of a perfectly conducting body, equal to zero. This guarantees a unique solution. In magnetostatics the boundary condition on the surface of a perfectly conducting body is that the normal component of the magnetic field should be zero and the choice of the image currents is dictated by this boundary condition. There are situations, however, in which, as we shall see below, the boundary condition is automatically satisfied independently of whether or not we introduce image currents. Before proceeding with this difficulty, we would like to draw an analogy between electrostatics and magnetostatics. In electrostatics the fundamental unit is the point charge which produces a Coulombic field. In magnetostatics the fundamental unit is the current element. The magnetic field, associated with it, is given by

$$\underline{dH} = \frac{1}{4\pi} \frac{i d\ell \times \underline{R}}{R^3} \quad (\text{A-1})$$

where $\underline{R} = \underline{r} - \underline{r}'$, \underline{r} is the observation point and \underline{r}' is the position vector of the current element. Actually steady current flows in closed loops and the claim is usually made that \underline{dH} given by (A-1) is only a mathematical convenience and the true observable field is obtained by integrating (A-1) over a closed loop. A fundamental difference between a field given by (A-1) and the field due to a closed loop is that $\nabla \times \underline{dH} \neq 0$ whereas $\nabla \times \oint \underline{dH} = 0$, as long as we observe at points away from the current source. Despite the fact that \underline{dH} is not curlfree we would like to construct a physical model for a current element and derive (A-1) as a consequence of Maxwell's equations. To preserve current continuity we have to assume that at the ends of the current element charge accumulates. Thus, at the ends we have $dQ_{\pm}/dt \mp i = 0$ or $Q_{\pm} = \pm it$. If we introduce the potentials \underline{A} and ϕ and choose the Lorentz gauge we find that the fields satisfying Maxwell's equation are given by

$$\underline{E} = -\nabla\phi - \frac{\partial \underline{A}}{\partial t} \quad (\text{A-2})$$

$$\mu_0 \underline{H} = \nabla \times \underline{A} \quad (\text{A-3})$$

where

$$\underline{A} = \frac{\mu_0}{4\pi} \int_V \frac{\underline{J}(\underline{r}', t - R/c)}{R} dV \quad (\text{A-4})$$

$$\phi = \frac{1}{4\pi\epsilon_0} \int_V \frac{\rho(\underline{r}', t - R/c)}{R} dV \quad (\text{A-5})$$

Assuming that the charges Q_{\pm} are point charges and recalling that i is a time independent current (A-4) and (A-5) give

$$d\underline{A} = \frac{\mu_0}{4\pi} \frac{id\underline{l}}{R} \quad (\text{A-6})$$

$$\begin{aligned} d\phi &= \frac{1}{4\pi\epsilon_0} \left\{ \frac{Q_+^{(\text{ret})}}{R_1} + \frac{Q_-^{(\text{ret})}}{R_2} \right\} \\ &= \frac{1}{4\pi\epsilon_0} \left\{ \frac{i(t - R_1/c)}{R_1} + \frac{-i(t - R_2/c)}{R_2} \right\} \\ &= \frac{it}{4\pi\epsilon_0} \left\{ \frac{1}{R_1} + \frac{-1}{R_2} \right\} \\ &= \frac{1}{4\pi\epsilon_0} \frac{\underline{p} \cdot \underline{R}}{R_3} \quad (\text{A-7}) \end{aligned}$$

where

$$\underline{p} = (it)d\underline{l}$$

We thus see that

$$\underline{dE} = - \nabla d\phi = - \nabla \frac{\underline{p} \cdot \underline{R}}{4\pi\epsilon_0 R^3} \quad (\text{A-8})$$

$$\underline{dH} = \frac{1}{4\pi} \frac{d\underline{l} \times \underline{R}}{R^3} \quad (\text{A-9})$$

We can easily verify, by using standard vectorial relations, that

$$\nabla \times \underline{dH} = \frac{\partial d\underline{D}}{\partial t}$$

which shows that despite its rotational character, \underline{dH} can still represent a physical magnetostatic field. We should also observe that despite the fact that the charges Q_{\pm} grow with time they only give rise to static-like electric field configurations. We then understand that at each moment we can treat the electric field configuration as static and apply the method of images. Once this is done the image current element arises automatically by satisfying current continuity. We conclude that the magnetostatic image problem can be associated with an electrostatic image problem and that the fields involved satisfy the time dependent Maxwell's equations. One can easily show that for plane perfectly conducting interfaces the normal component of the total magnetic field is also zero. We will show below that this is also the case for a current element parallel to the surface of a perfectly conducting sphere. To show the value of our novel way of treating current elements consider the situation of a current element, along the z-axis, above a perfectly conducting plane interface perpendicular to the z-axis. Using (A-1) one can easily conclude that H_z due to the current element on the interface is zero. The image, if any, should also be along the z-axis, but there is no way to determine its relative position or strength since the total H_z on the interface will be always zero. In the electrostatic case such a problem never arises. According to our method the current element is always accompanied by the Q_+ and Q_- charges which makes possible the exact determination of the image current element.

Consider now a current element $i_1 d\underline{l}_1$ parallel to the surface of a perfectly conducting sphere of radius b . We choose the x axis along the

direction of the current element $i_1 d\ell_1$ situated at the point P_1 with a position vector \underline{r}_1 along the z-axis (see fig. 4). The image current element will be directed along the negative x-axis and its position vector is \underline{r}_2 . We will assume according to the well-known situation in electrostatics that $|\underline{r}_2| = b^2/a$ where $|\underline{r}_1| = a$. We will show that the total H_r at any point P' on the sphere is zero provided that $i_1 d\ell_1 / i_2 d\ell_2 = a/b$ (in accordance with the associated electrostatic problem). We have

$$d\underline{H}_1 = \frac{i_1}{4\pi} \frac{i_1 d\ell_1 \times \underline{R}_1}{R_1^3} = \frac{i_1 d\ell_1}{4\pi} \frac{(\hat{a}_x) \times \underline{R}_1}{R_1^3} \quad (\text{A-10})$$

$$d\underline{H}_2 = \frac{i_2}{4\pi} \frac{i_2 d\ell_2 \times \underline{R}_2}{R_2^3} = - \frac{i_2 d\ell_2}{4\pi} \frac{(\hat{a}_x) \times \underline{R}_2}{R_2^3} \quad (\text{A-11})$$

The r-component is

$$\begin{aligned} dH_r &= \hat{a}_r \cdot (d\underline{H}_1 + d\underline{H}_2) \\ &= \hat{a}_r \cdot \left[\frac{i_1 d\ell_1 [y \hat{a}_z - \hat{a}_y (z-a)]}{[x^2 + y^2 + (z-a)^2]^{3/2}} - \frac{i_2 d\ell_2 [y \hat{a}_z - \hat{a}_y (z-b^2/a)]}{[x^2 + y^2 + (z-b^2/a)^2]^{3/2}} \right] \end{aligned} \quad (\text{A-12})$$

We can easily see that

$$x^2 + y^2 + (z-a)^2 = b^2 + a^2 - 2az$$

$$x^2 + y^2 + (z - b^2/a)^2 = \left(\frac{b}{a}\right)^2 [b^2 + a^2 - 2az]$$

and (A-12) gives

$$dH_r = \frac{1}{(b^2 + a^2 - 2az)^{3/2}} (\hat{a}_r \cdot \hat{a}_y) (i_1 d\ell_1 a - i_2 d\ell_2 \left(\frac{a}{b}\right)^3 \frac{b^2}{a})$$

Thus if $i_1 d\ell_1 / i_2 d\ell_2 = a/b$ we find $dH_r = 0$. From the geometry we understand that $d\ell_1/a = d\ell_2/b^2/a$ and consequently $i_1/i_2 = b/a$. Thus the image current i_2 is a/b larger than the original current i_1 in contrast to the electrostatic

situation in which the image charge is b/a smaller than the original charge. If instead of an element we have a current loop of radius "a" surrounding the sphere, the image loop will have a radius b^2/a and a current equal to $(a/b)i_1$ will flow in this loop. We can also demonstrate this situation in the following way. The field H_r due to the outer loop is given by

$$\begin{aligned}
 (r < a) \quad H_r &= -\frac{i_1}{2a} \sum_{\substack{n=1 \\ \text{odd}}}^{\infty} (-1)^{\frac{n+1}{2}} \frac{1.3.5\dots n(n+1)}{2.4.6\dots (n-1)(n+1)} \left(\frac{r}{a}\right)^{n-1} P_n(\cos \theta) \\
 &= -\frac{i_1}{2a} \sum_{\substack{n=1 \\ \text{odd}}}^{\infty} S_n \left(\frac{r}{a}\right)^{n-1} P_n(\cos \theta) \tag{A-13}
 \end{aligned}$$

The scattered field outside the sphere is curlfree and can be calculated as $\underline{H}_{sc} = -\nabla\phi$ where ϕ satisfies Laplace's equation. Thus

$$\begin{aligned}
 \phi &= \sum_{n=1}^{\infty} A_n r^{-(n+1)} P_n(\cos \theta) \\
 (H_{sc})_r &= -\frac{\partial\phi}{\partial r} = \sum_{n=1}^{\infty} A_n (n+1) r^{-(n+2)} P_n(\cos \theta) \tag{A-14}
 \end{aligned}$$

The boundary condition $(H_r)_{total} = 0$ at $r = b$ is satisfied if

$$A_n (n+1) b^{-(n+2)} = \frac{i_1}{2a} S_n \left(\frac{b}{a}\right)^{n-1},$$

and consequently

$$(H_{sc})_r = \frac{i_1}{2a} \sum_{\substack{n=1 \\ \text{odd}}}^{\infty} S_n \left(\frac{b}{a}\right)^{n-1} r^{-(n+2)} P_n(\cos \theta) b^{(n+2)} \tag{A-15}$$

(A-15) can be rewritten as

$$(H_{sc})_r = -\frac{i_2}{2(b^2/a)} \sum_{\substack{n=1 \\ \text{odd}}}^{\infty} S_n \left(\frac{b^2/a}{r}\right)^{n+2} P_n(\cos \theta) \tag{A-16}$$

where $i_2 = i_1 (a/b)$. (A-16) can be recognized as the H_r field of a loop of radius b^2/a and a current $i_1 (a/b)$ evaluated at $r = b > b^2/a$. The current i_2 flows opposite to the original current i_1 .

We would now like to emphasize that the analysis in this appendix dealt with the determination of images for current elements and is not restricted to the previous example where the sphere is surrounded by a circular current loop. In particular when the inclination angle ξ_1 is different from zero we can obtain images in a pointwise manner to obtain the situation depicted in figure 2.

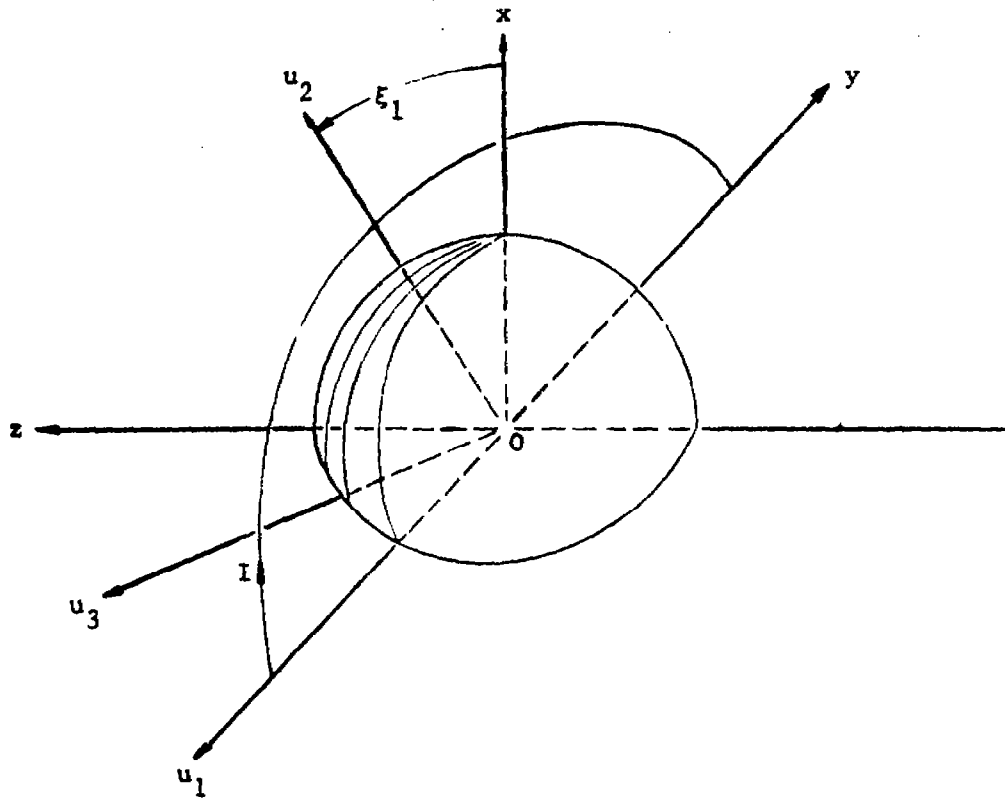


Figure 1. Simulator-Hemisphere geometry.

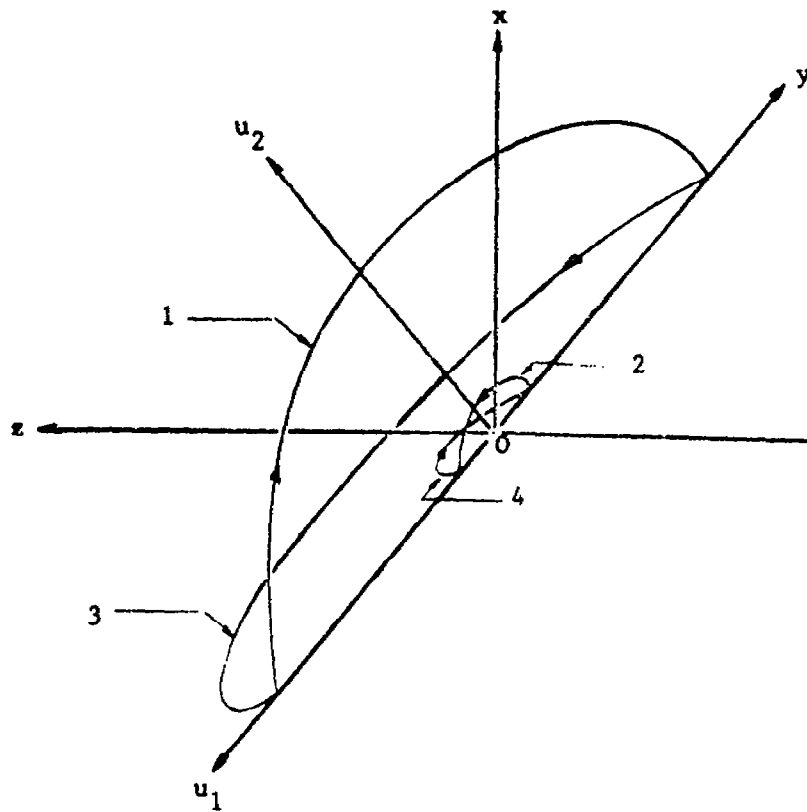


Figure 2. The four current half loops.

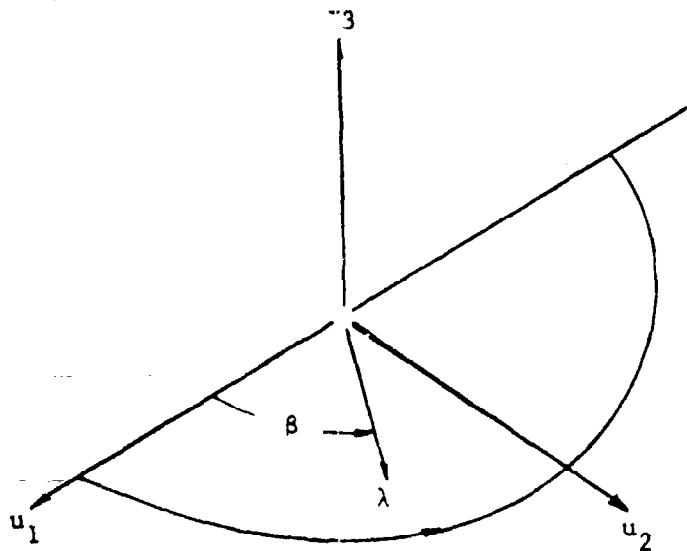


Figure 3. The coordinate systems (u_1, u_2, u_3) and (λ, β, u_3) associated with a typical half loop.

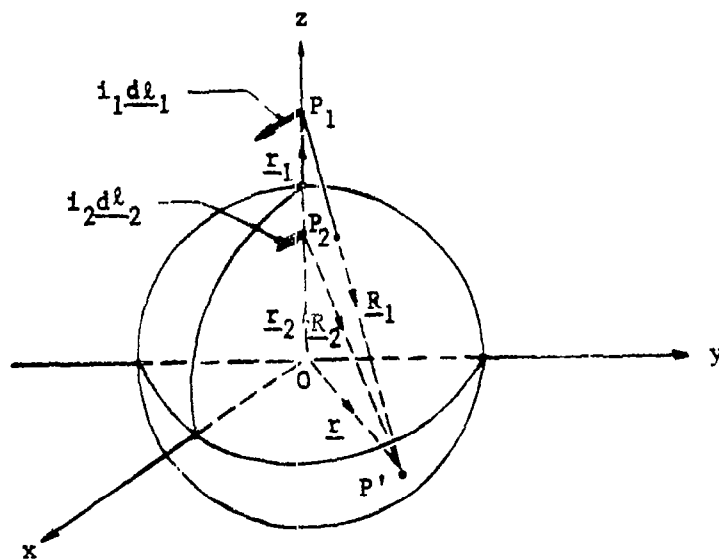
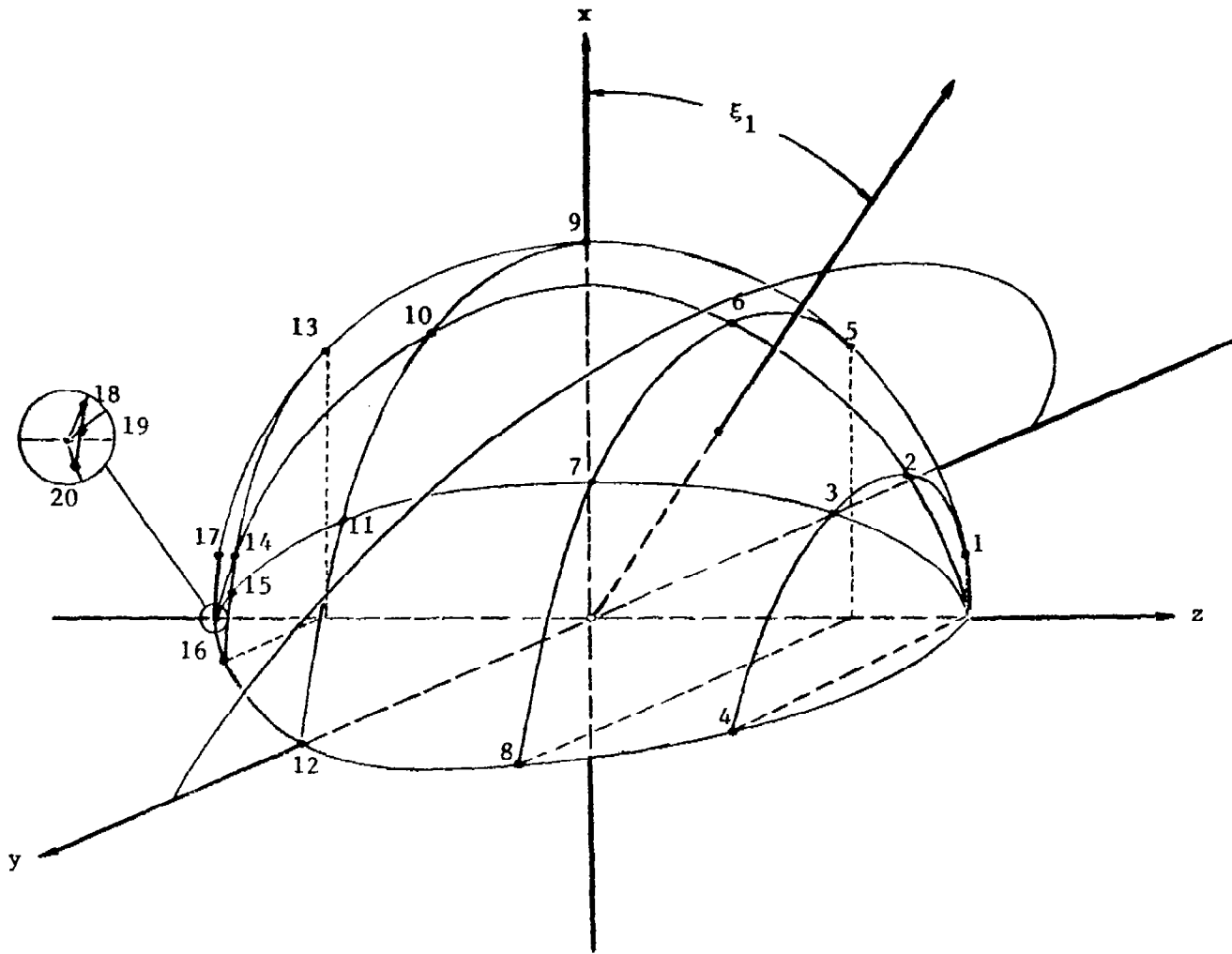


Figure 4. Image of a current element with respect to a perfectly conducting sphere. $(OP_1) = r_1$, $(OP_2) = r_2$.



20

Figure 5. Numbers 1 to 20 correspond to points on the hemisphere at which plots of $|h_\theta/h_{\theta L}|$, $|h_\phi/h_{\phi L}|$ and D were considered. 1, 2, 3, 4 ($\theta = \pi/20, \phi = 0, \pi/6, \pi/3, \pi/2$); 5, 6, 7, 8 ($\theta = \pi/4, \phi = 0, \pi/6, \pi/3, \pi/2$); 9, 10, 11, 12 ($\theta = \pi/2, \phi = 0, \pi/6, \pi/3, \pi/2$); 13, 14, 15, 16 ($\theta = 3\pi/4, \phi = 0, \pi/6, \pi/3, \pi/2$); 17, 18, 19, 20 ($\theta = 19\pi/20, \phi = 0, \pi/6, \pi/3, \pi/2$).

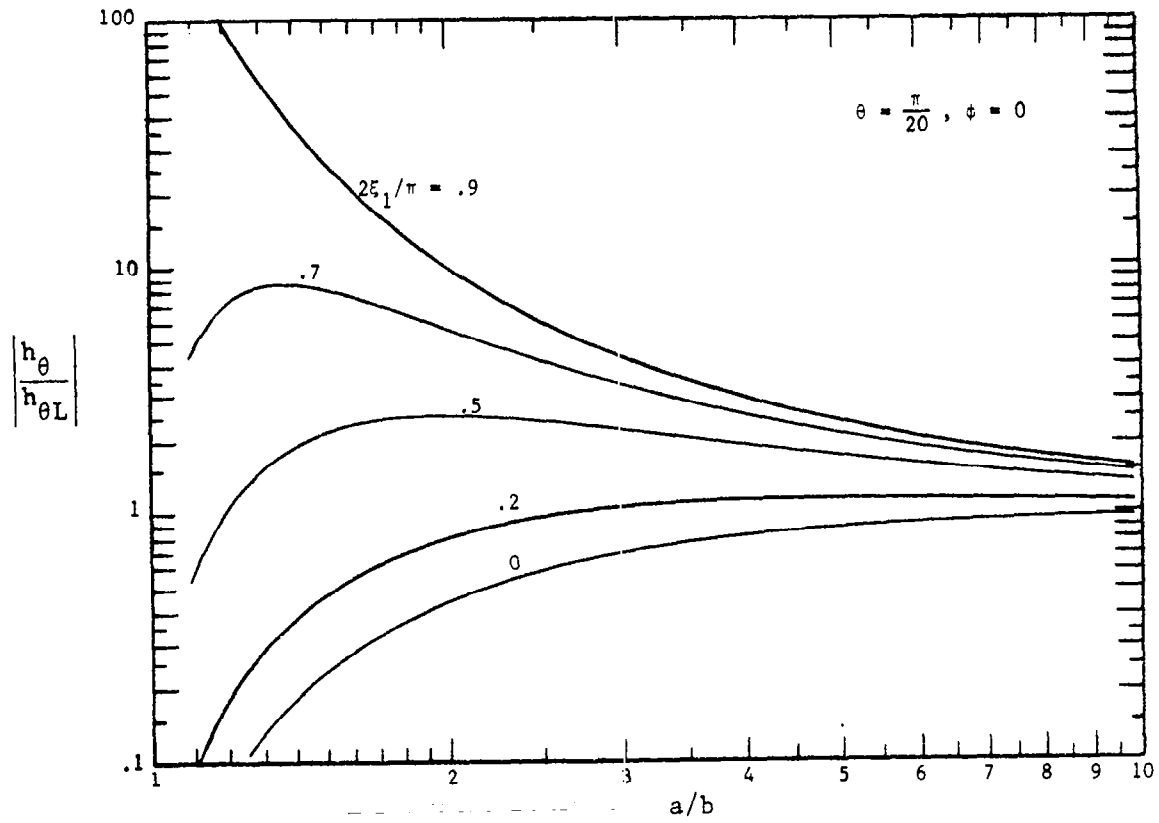


FIGURE 6

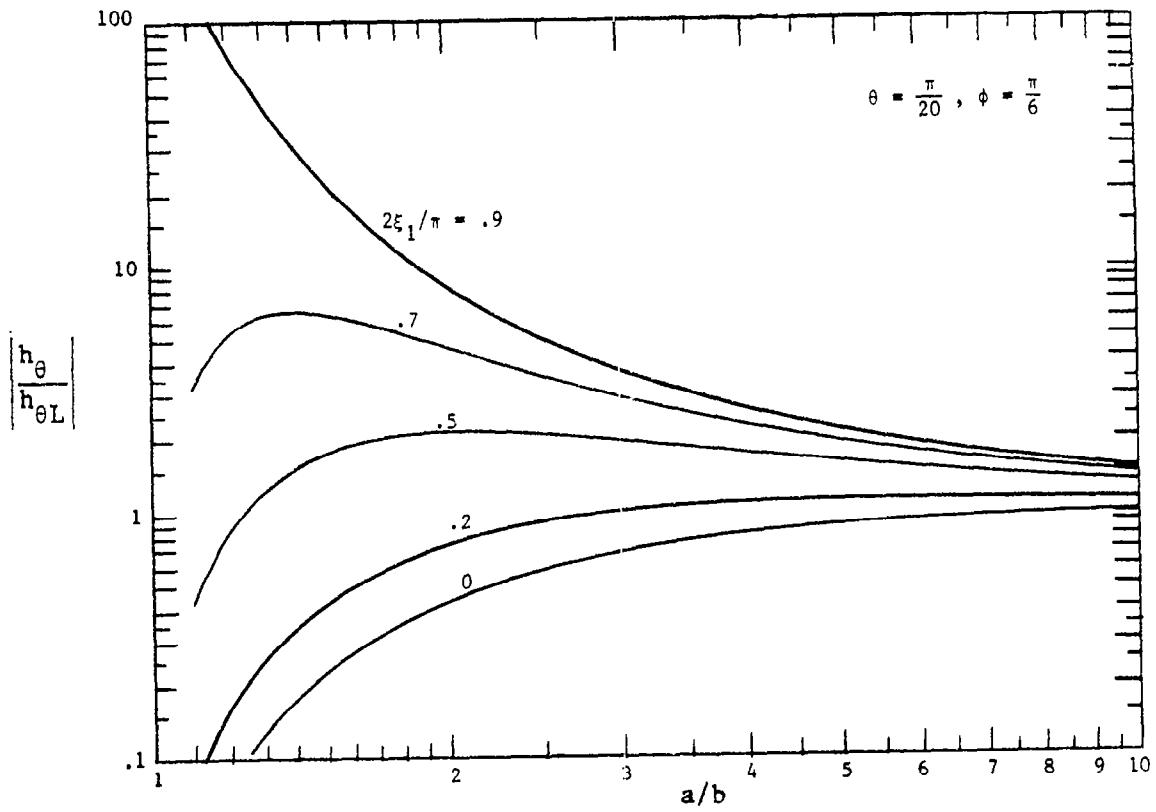


FIGURE 7

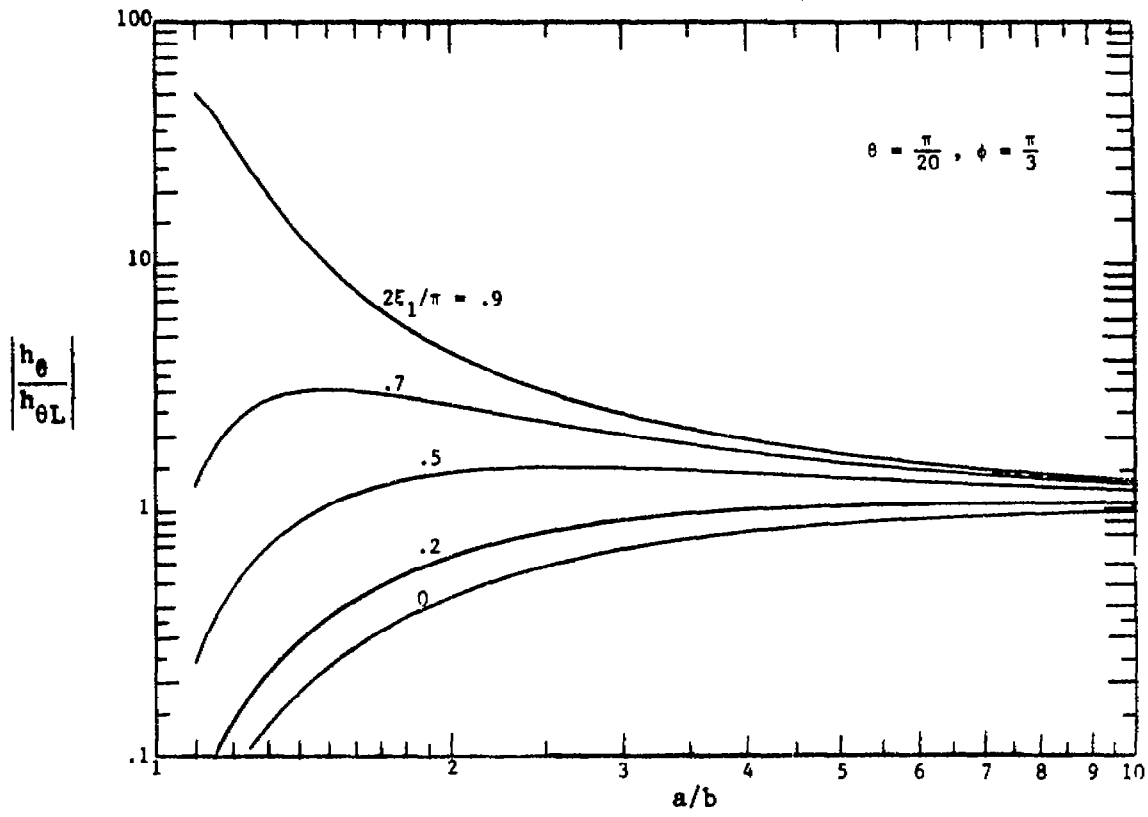


FIGURE 8

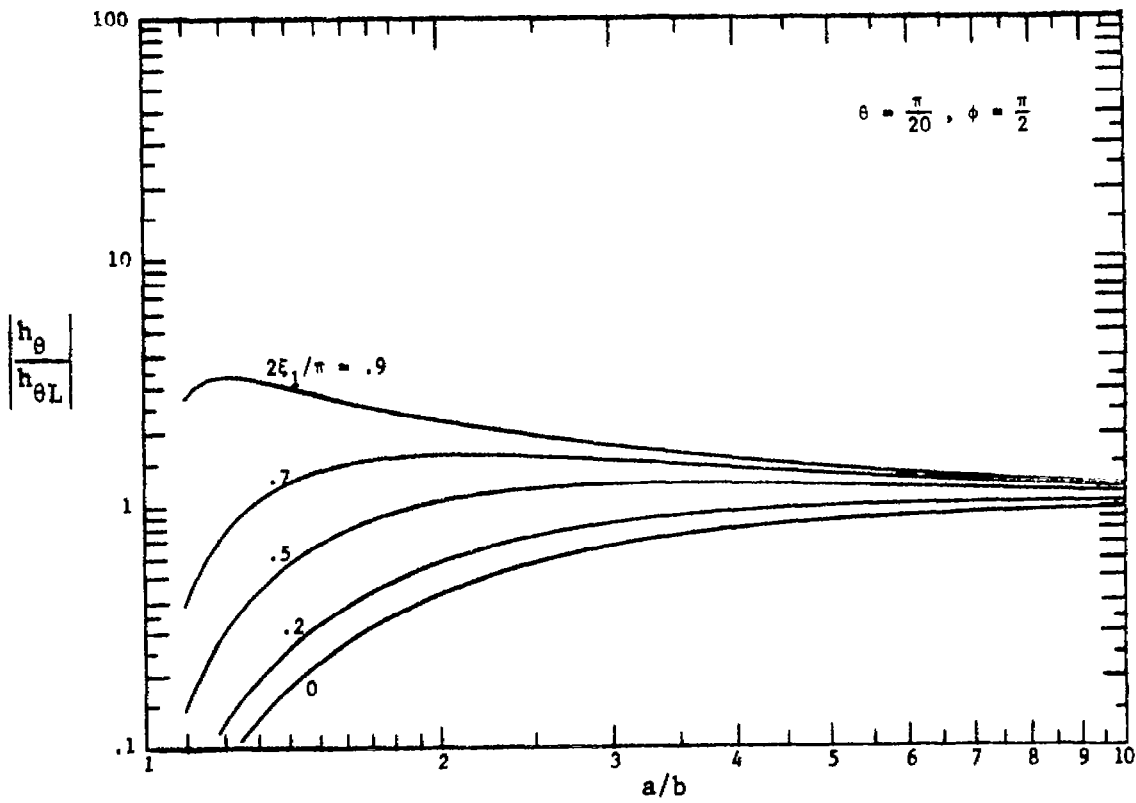


FIGURE 9

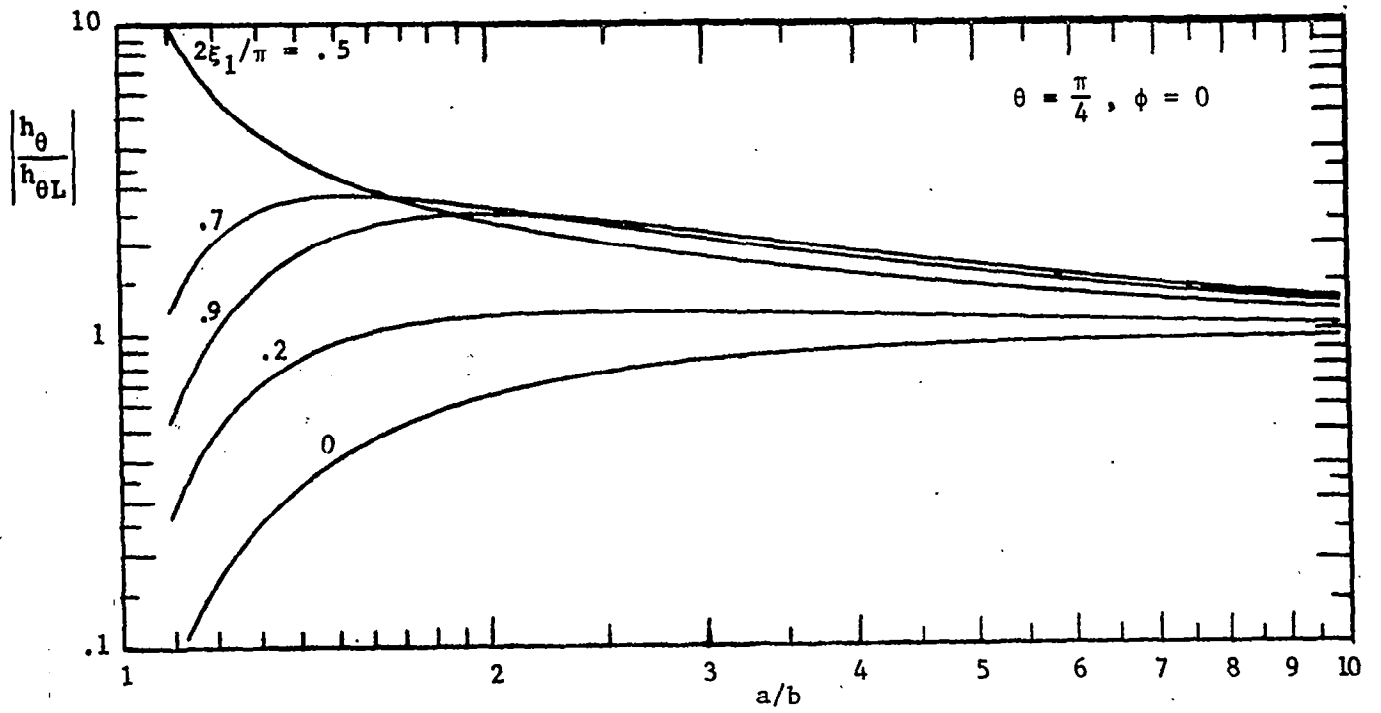


FIGURE 10

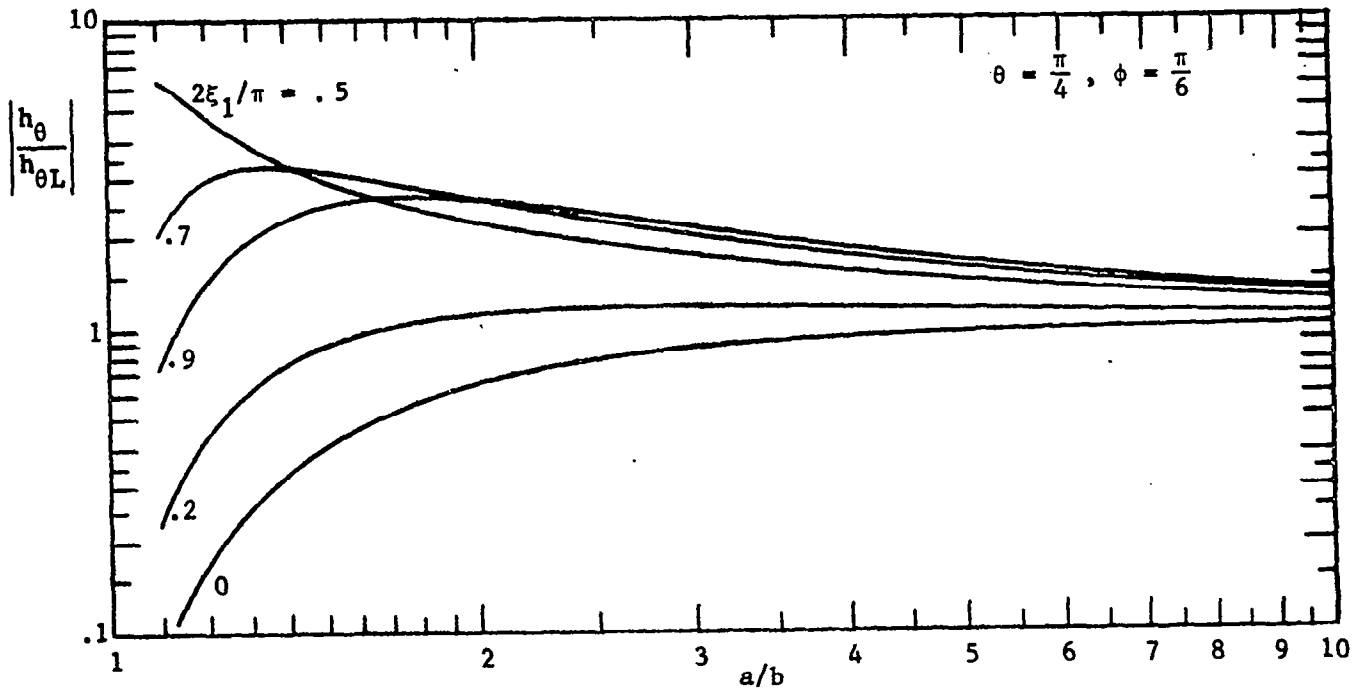


FIGURE 11

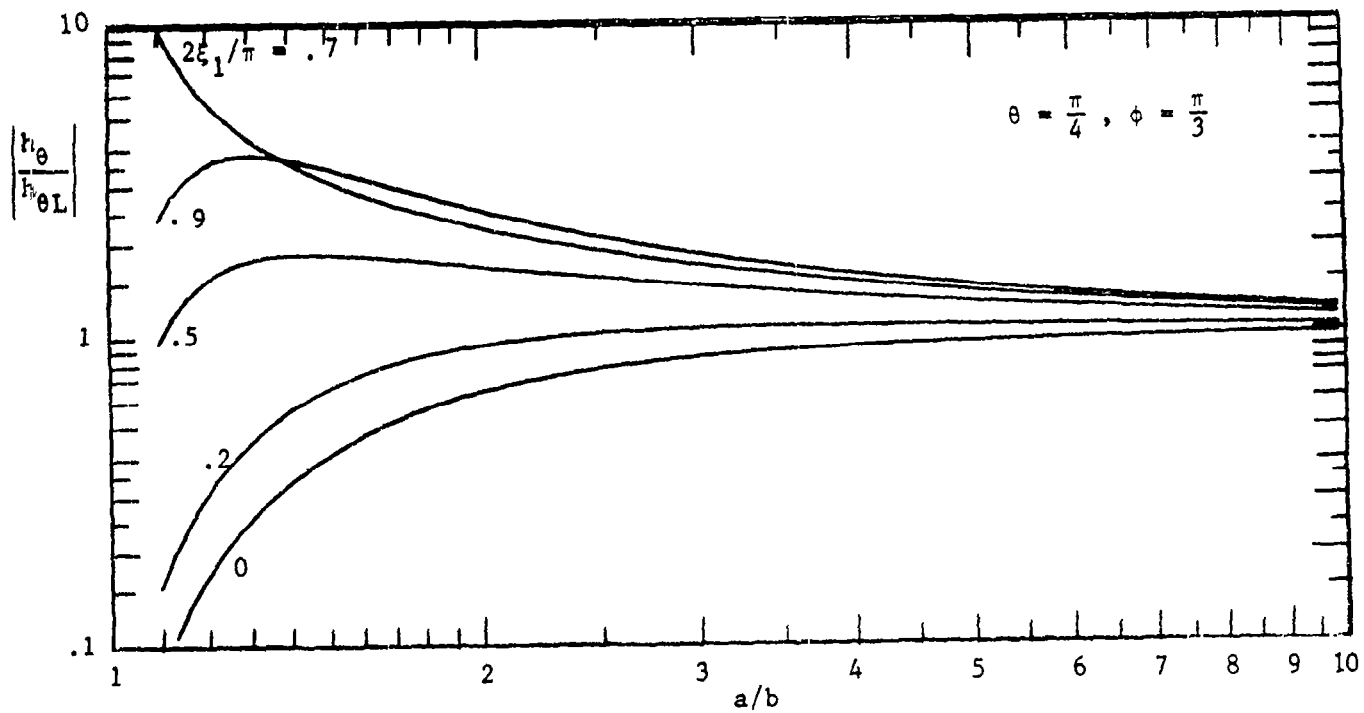


FIGURE 12

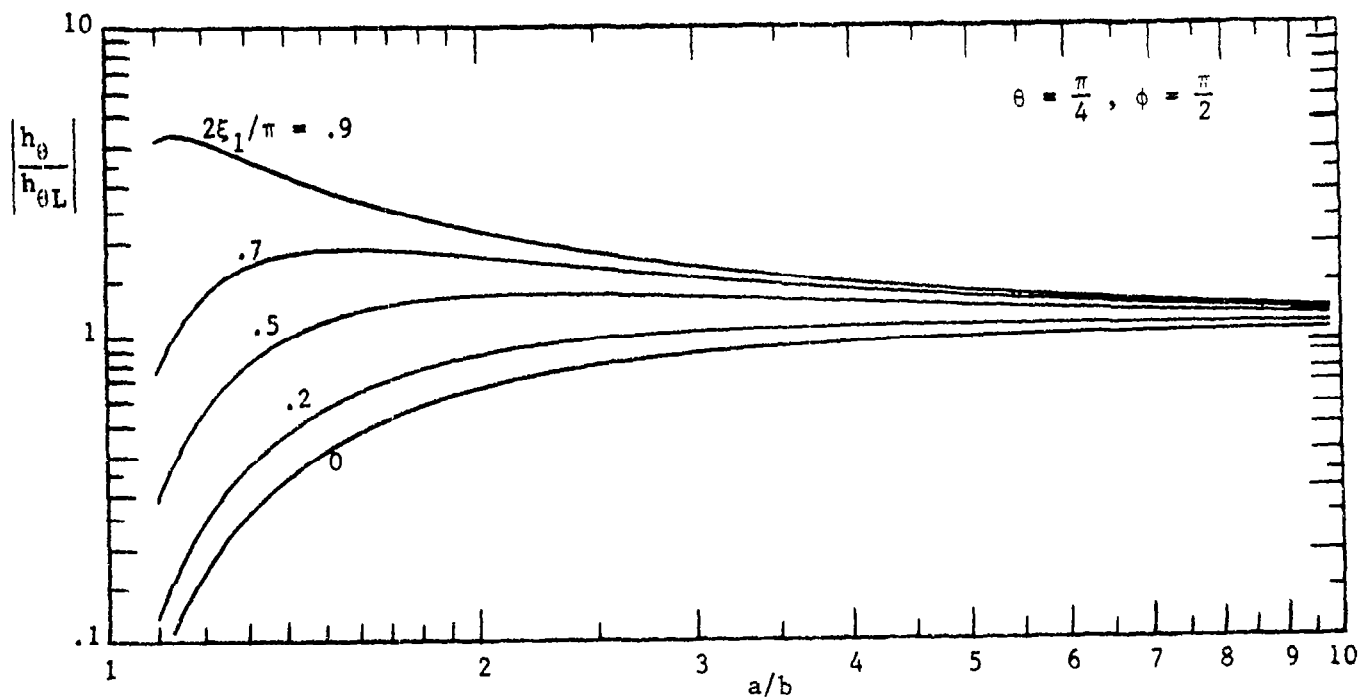


FIGURE 13

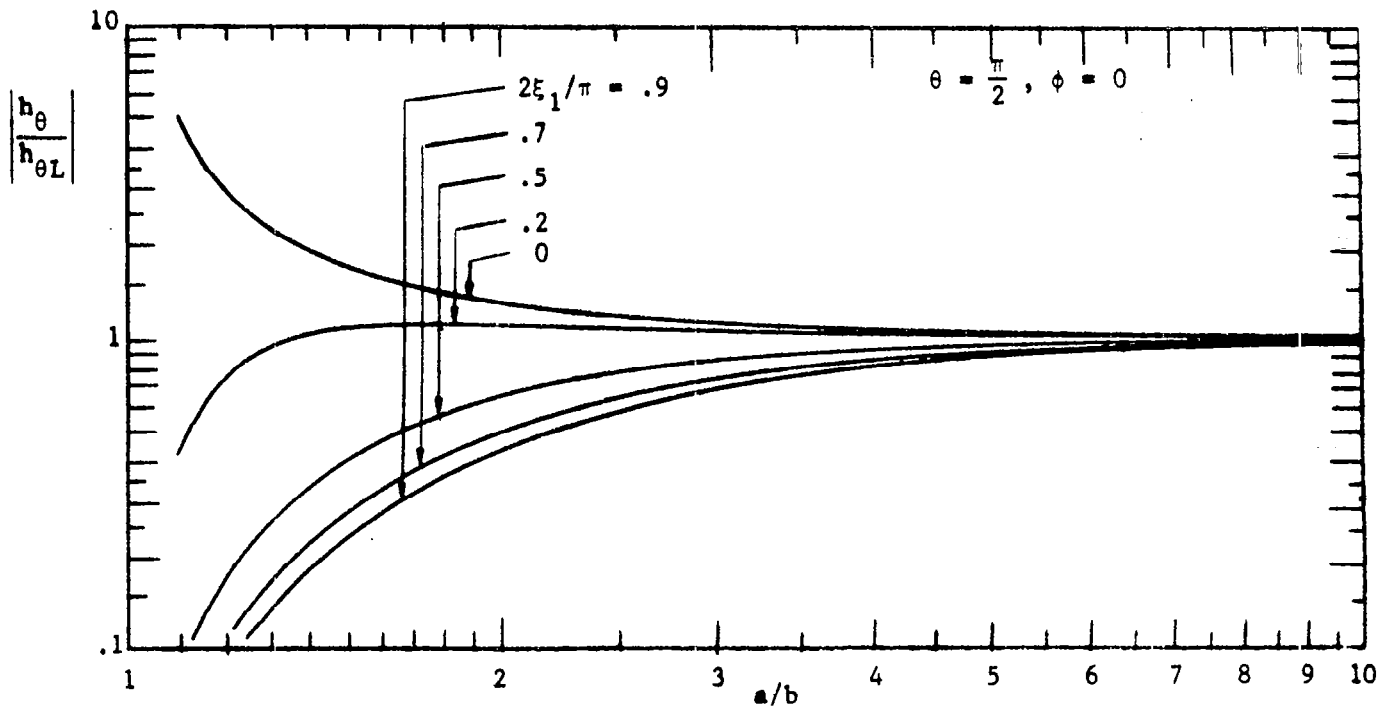


FIGURE 14

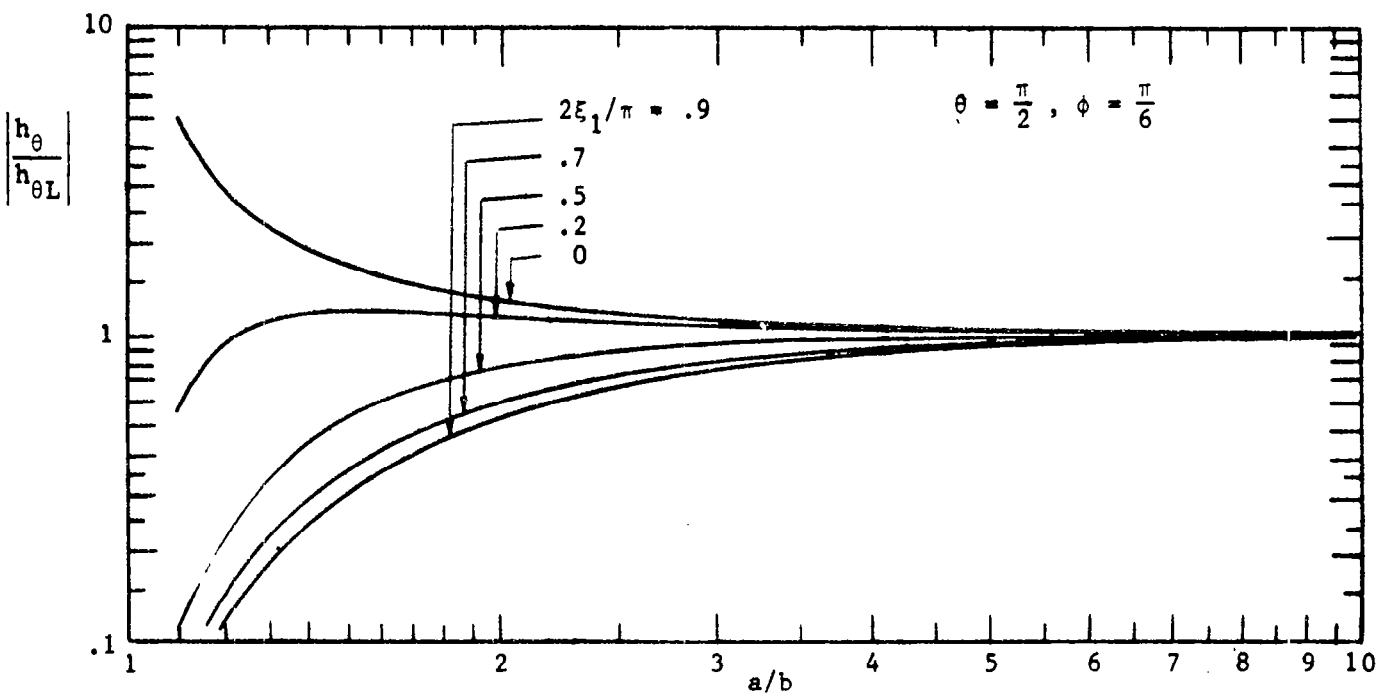


FIGURE 15

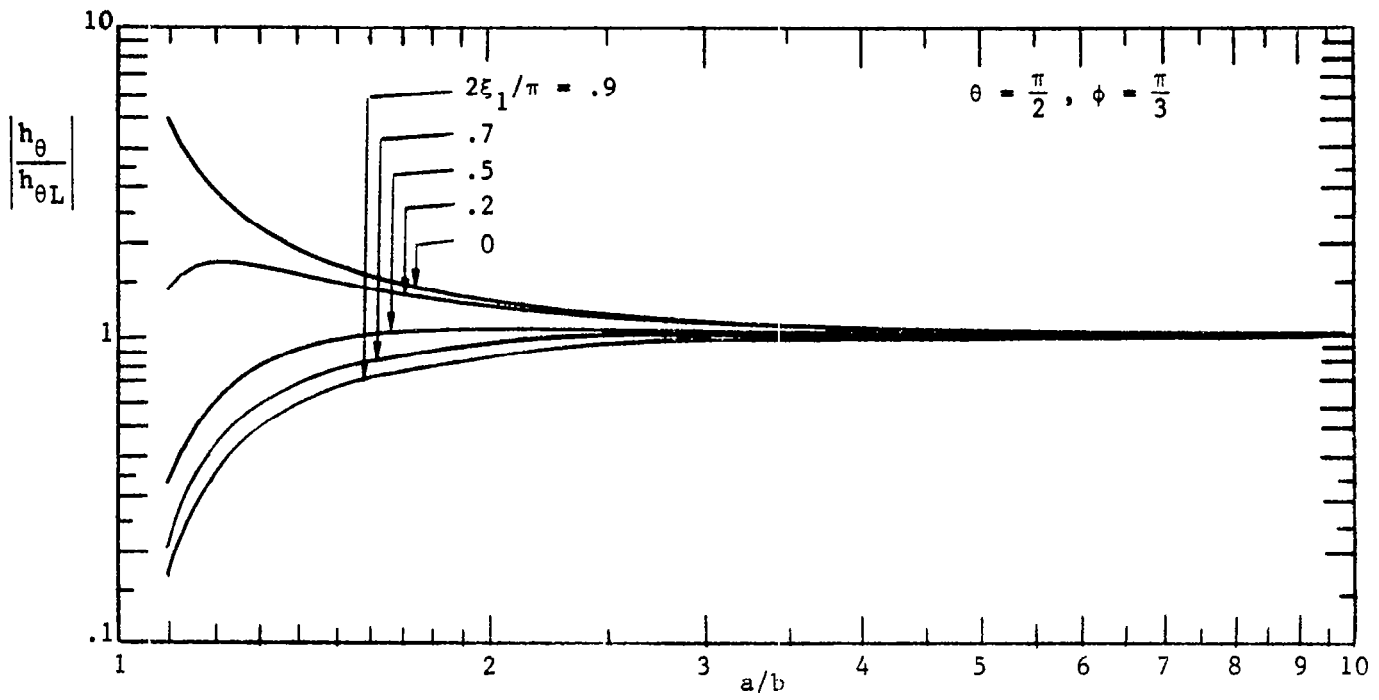


FIGURE 16

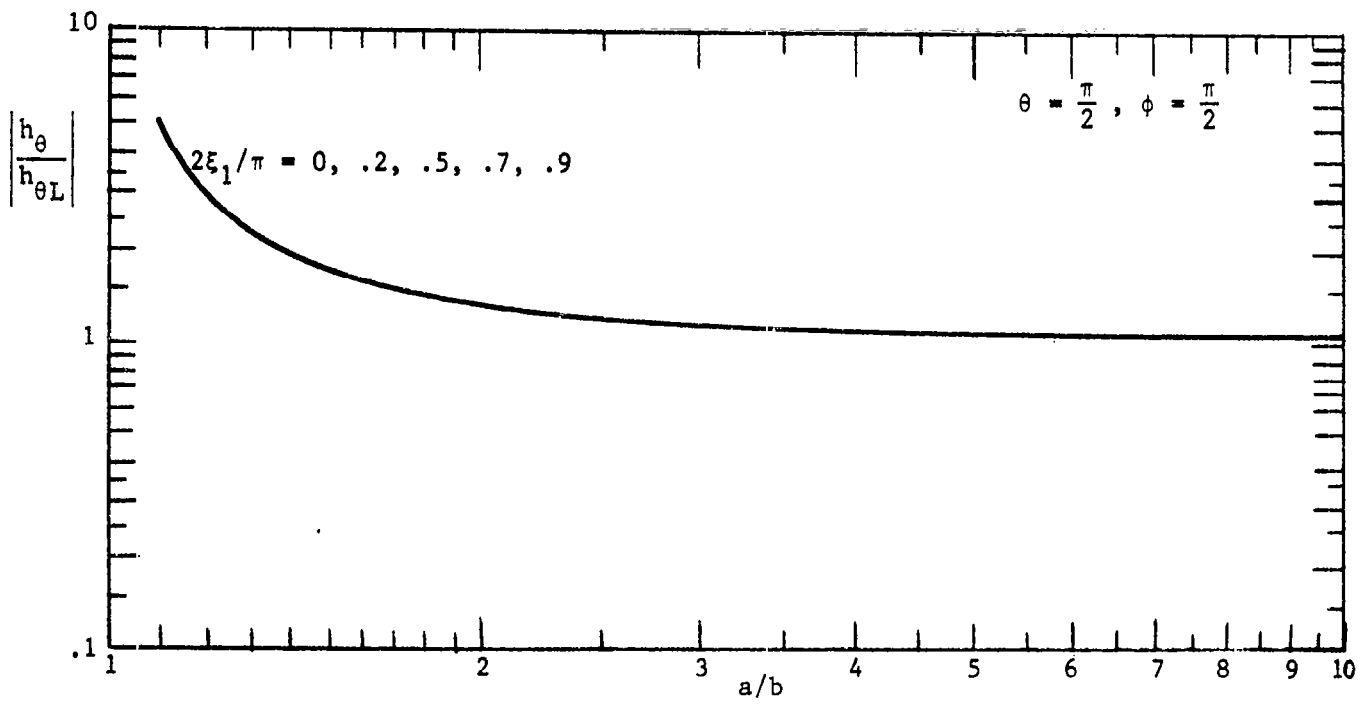


FIGURE 17

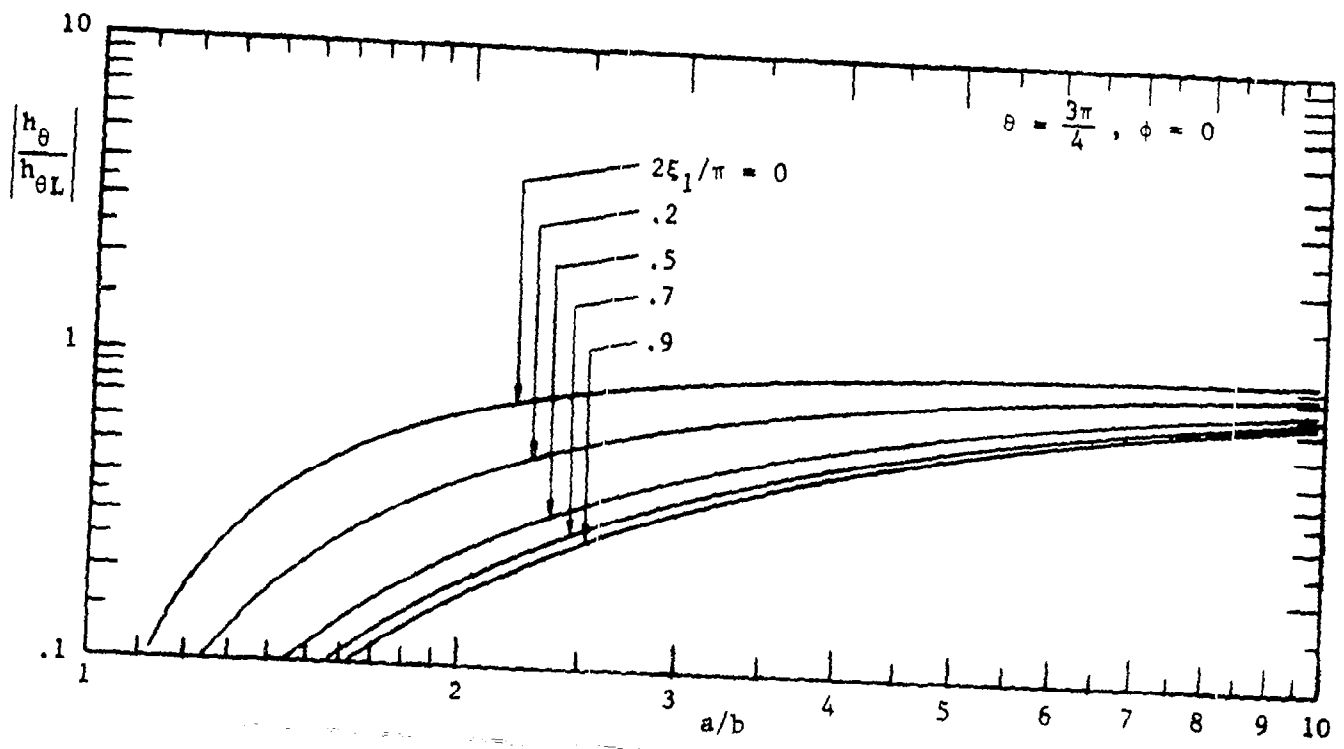


FIGURE 18

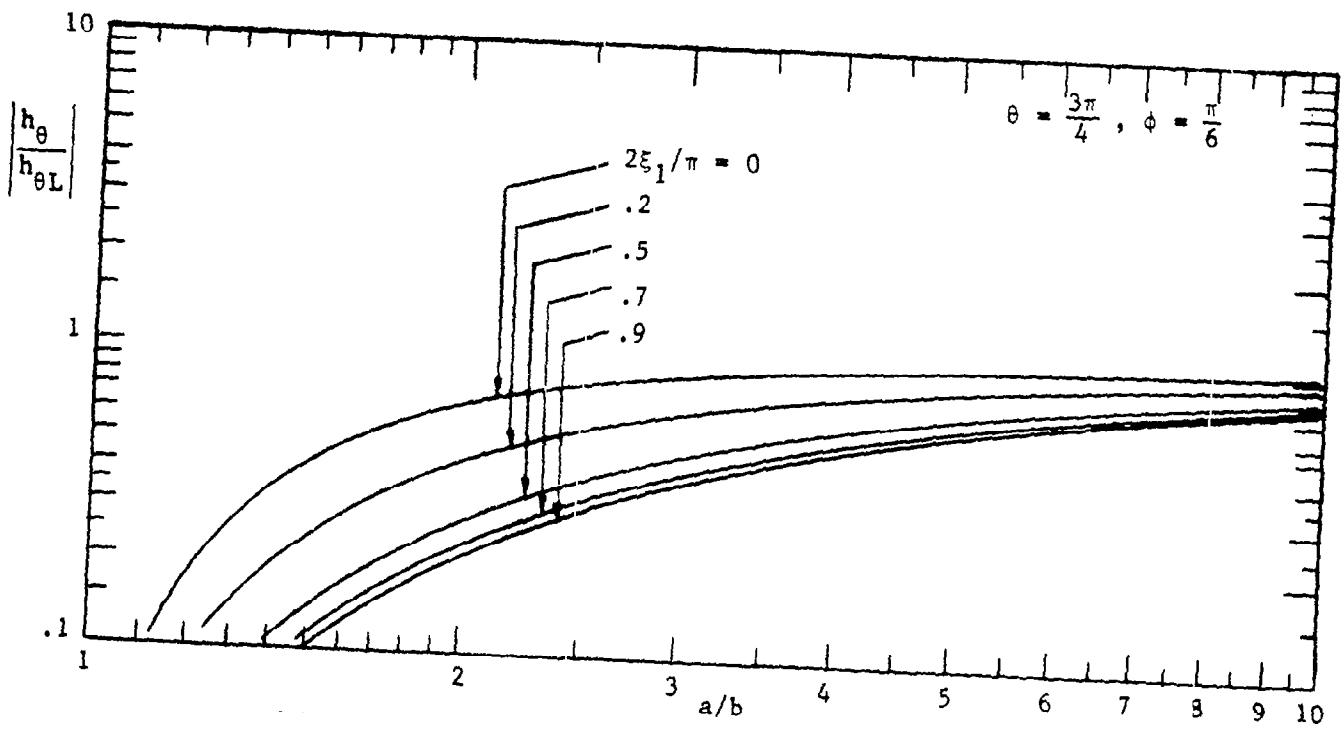


FIGURE 19

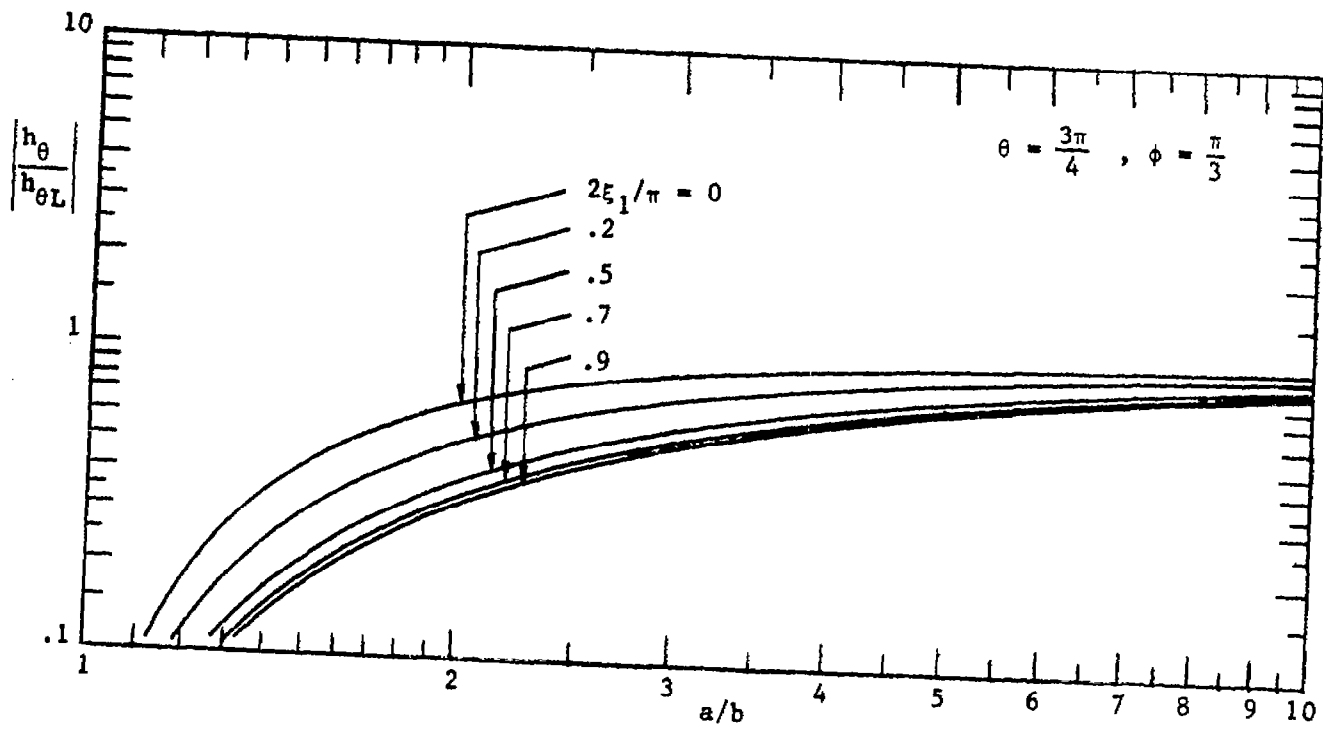


FIGURE 20

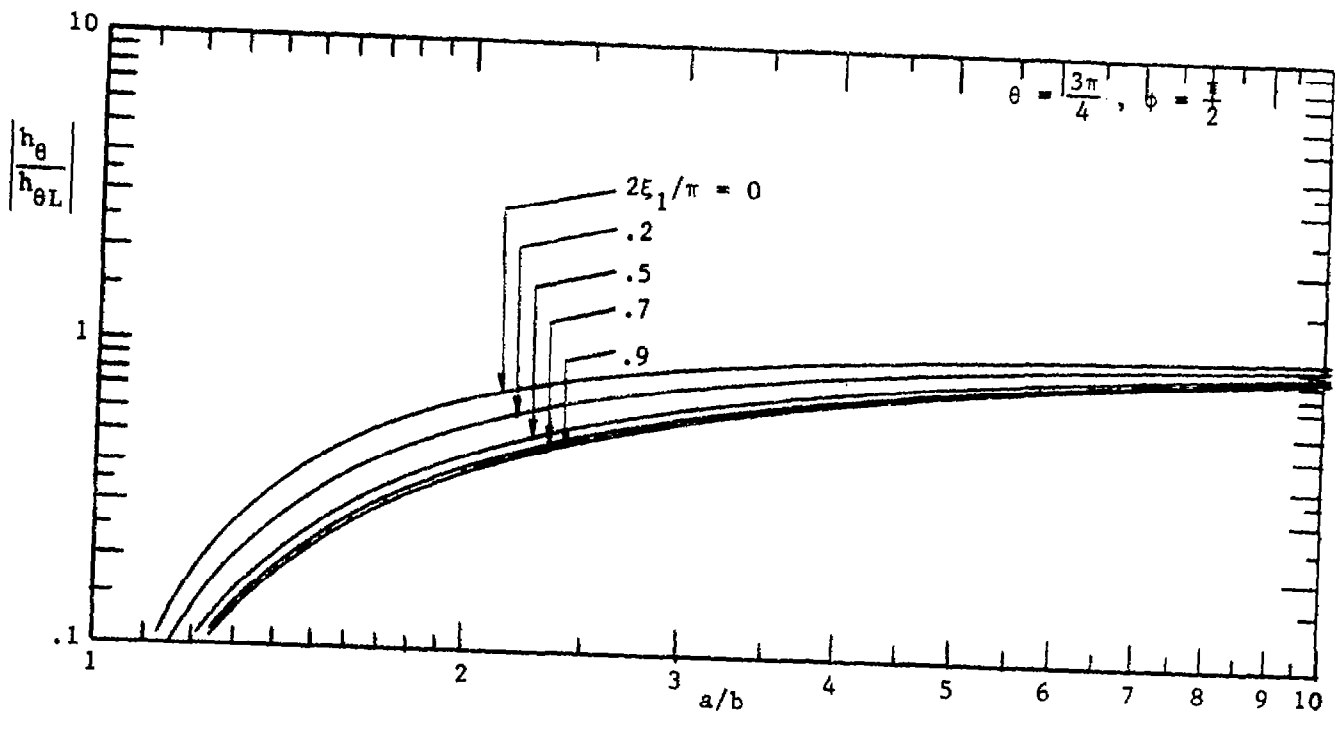


FIGURE 21

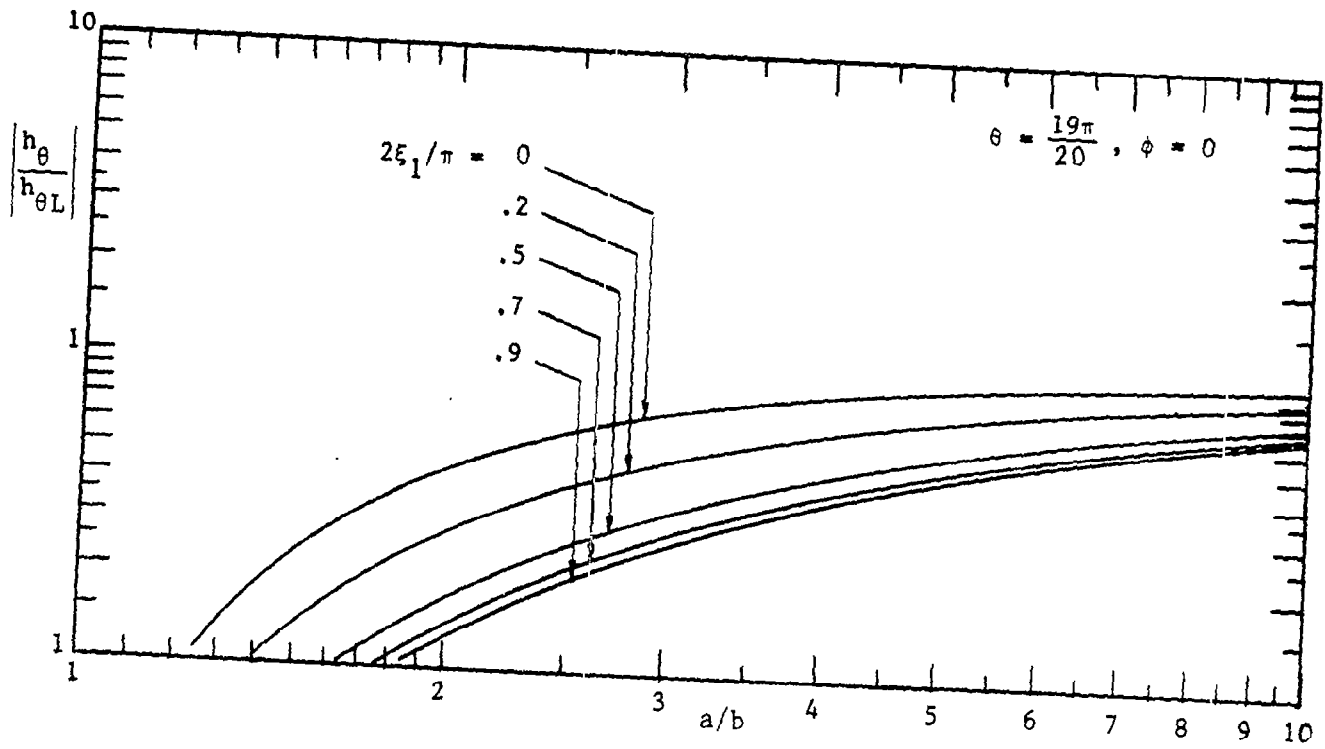


FIGURE 22

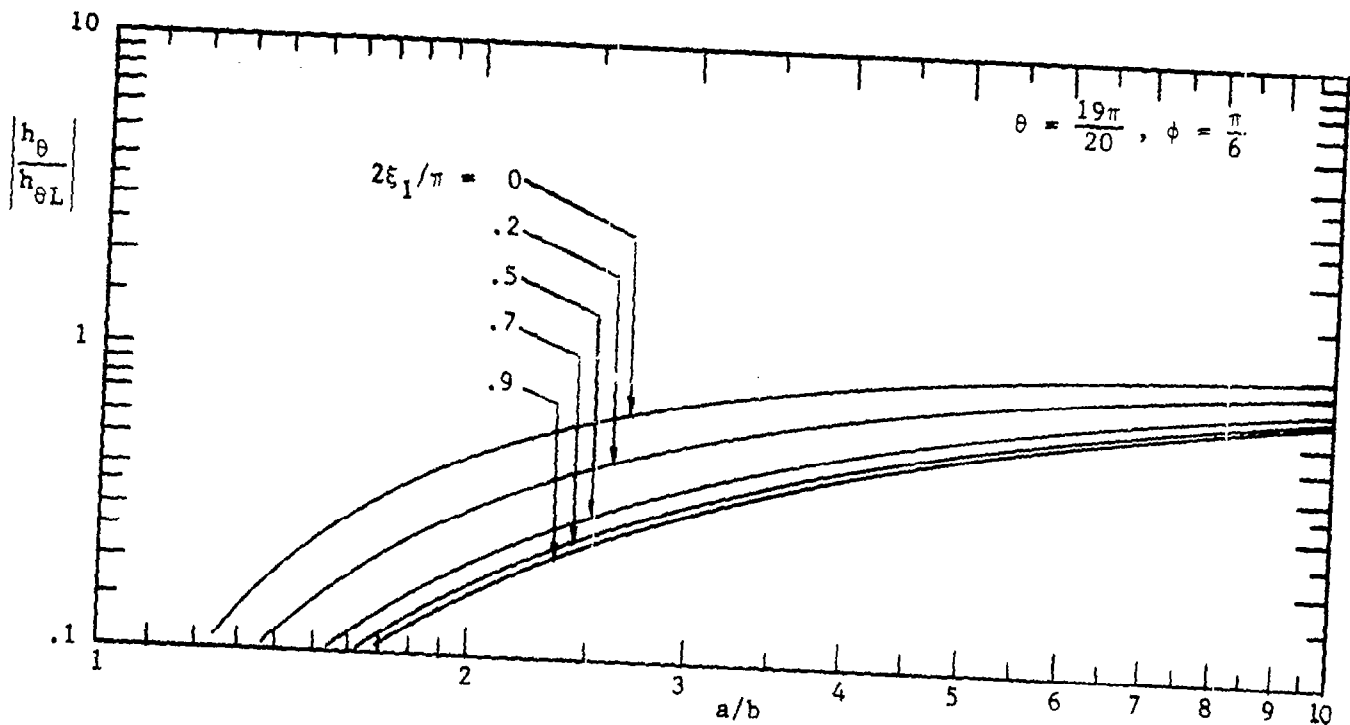


FIGURE 23

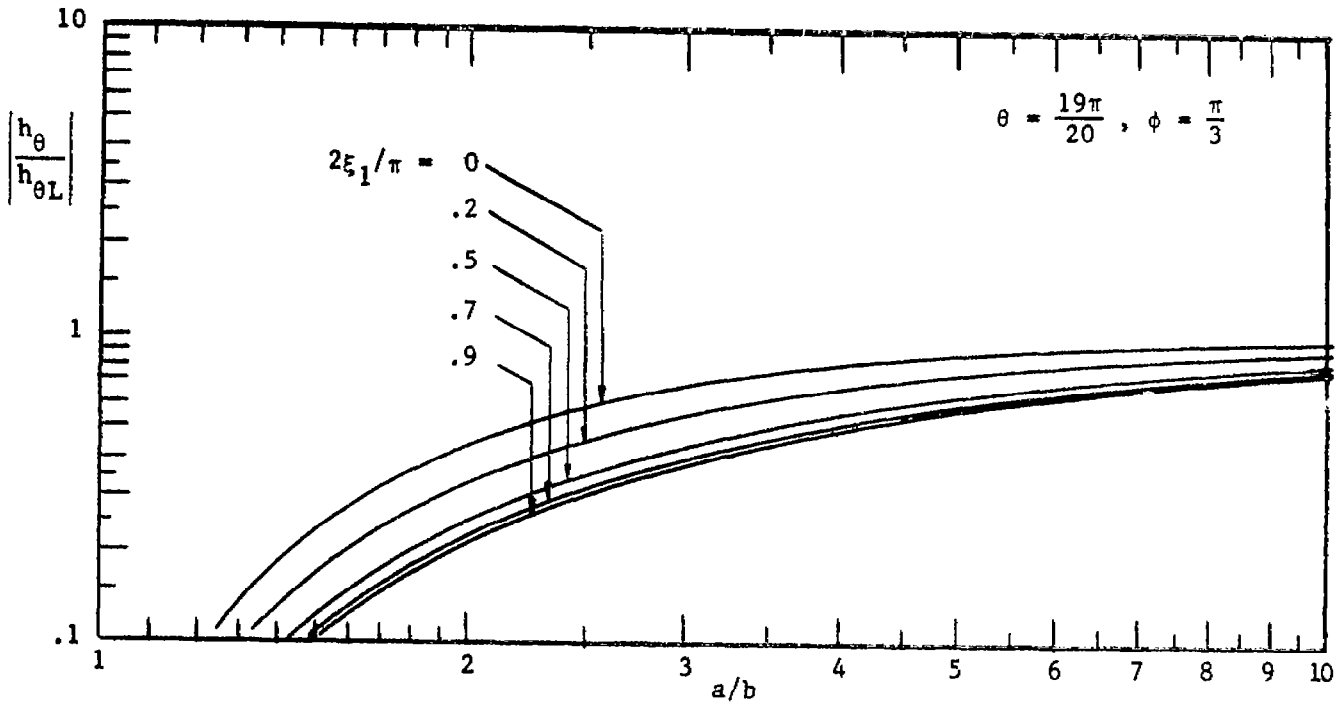


FIGURE 24

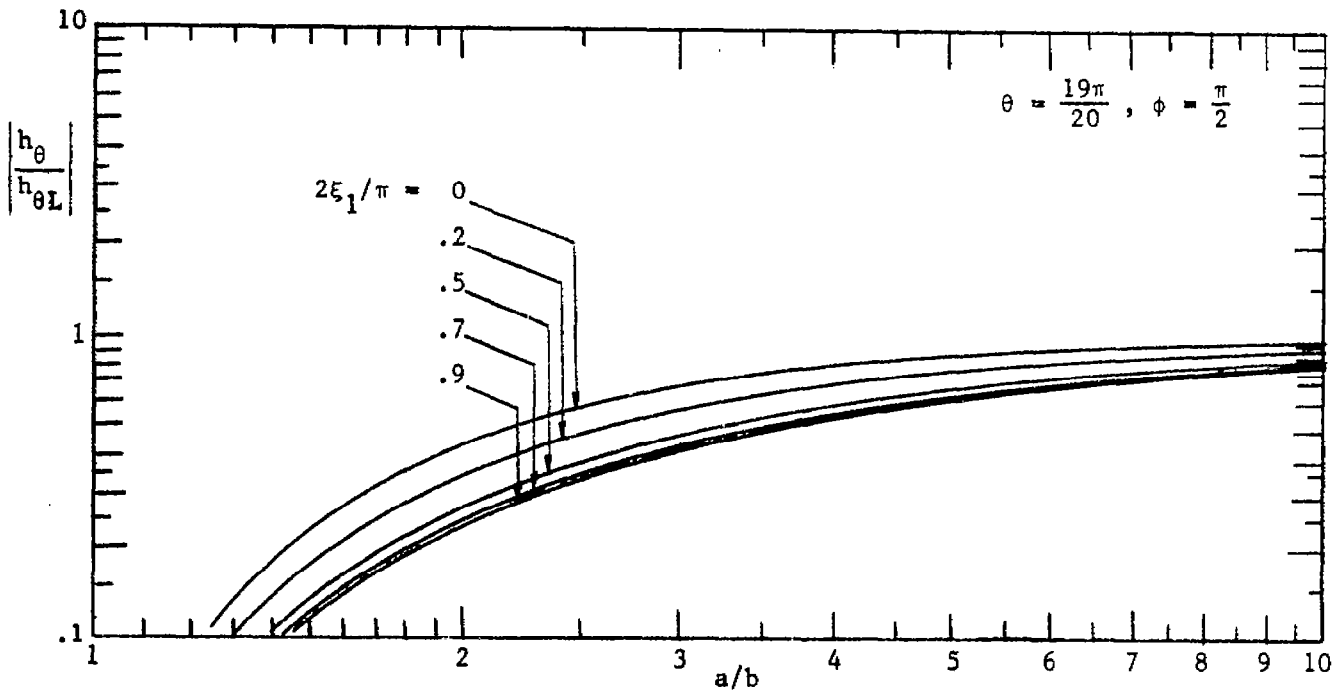


FIGURE 25

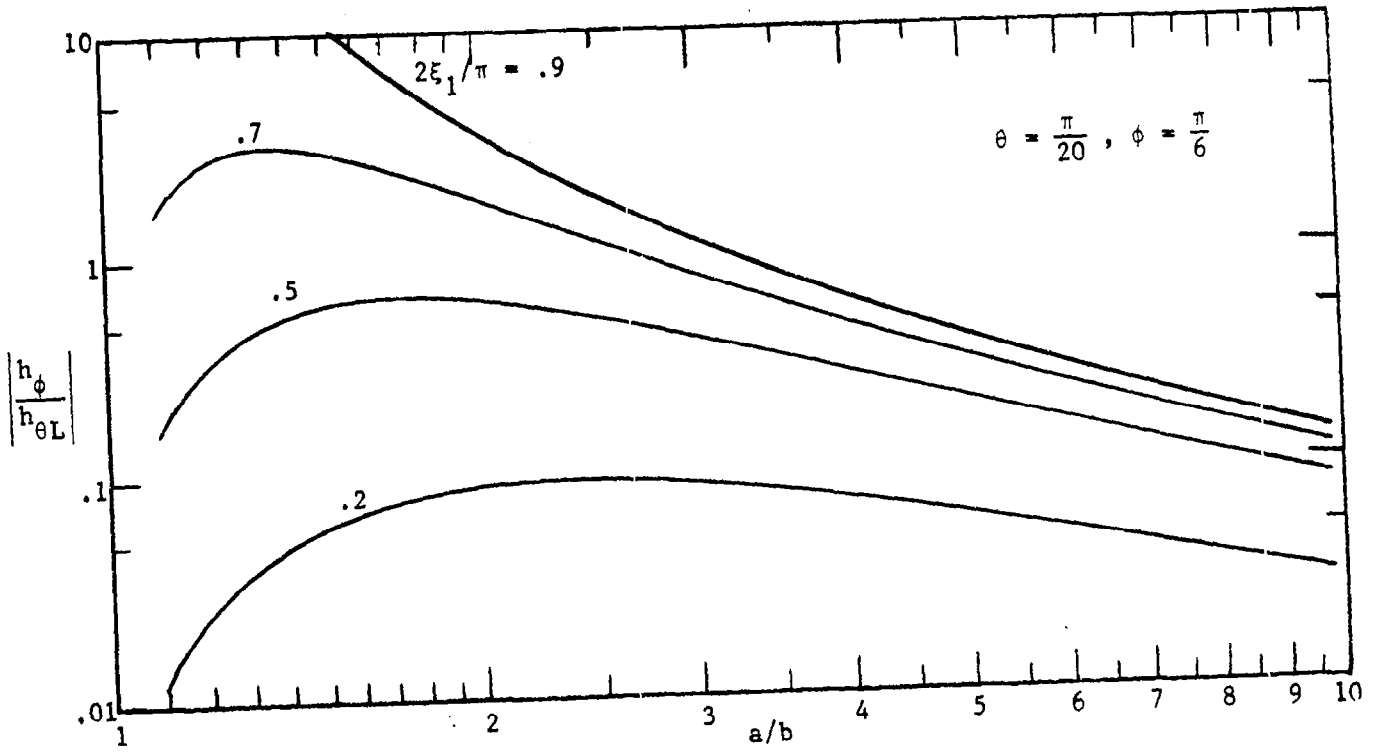


FIGURE 26

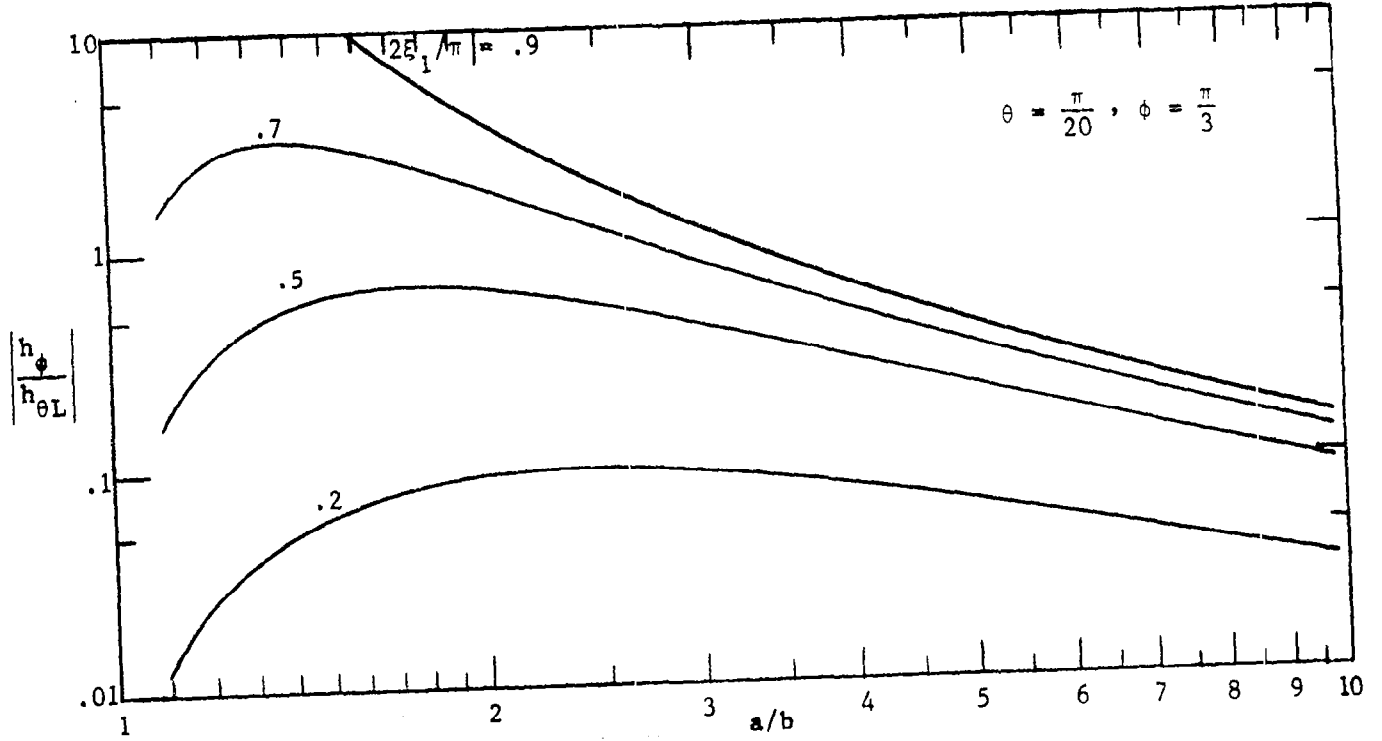


FIGURE 27

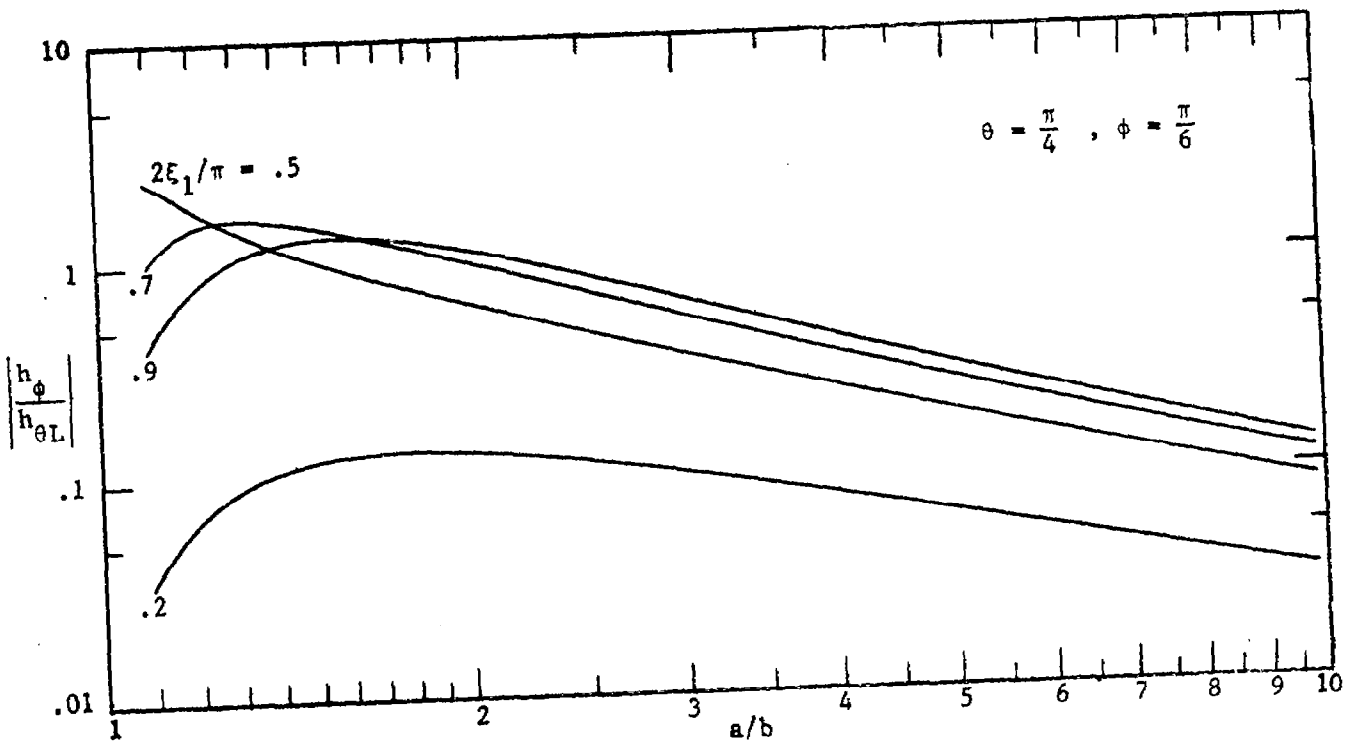


FIGURE 28

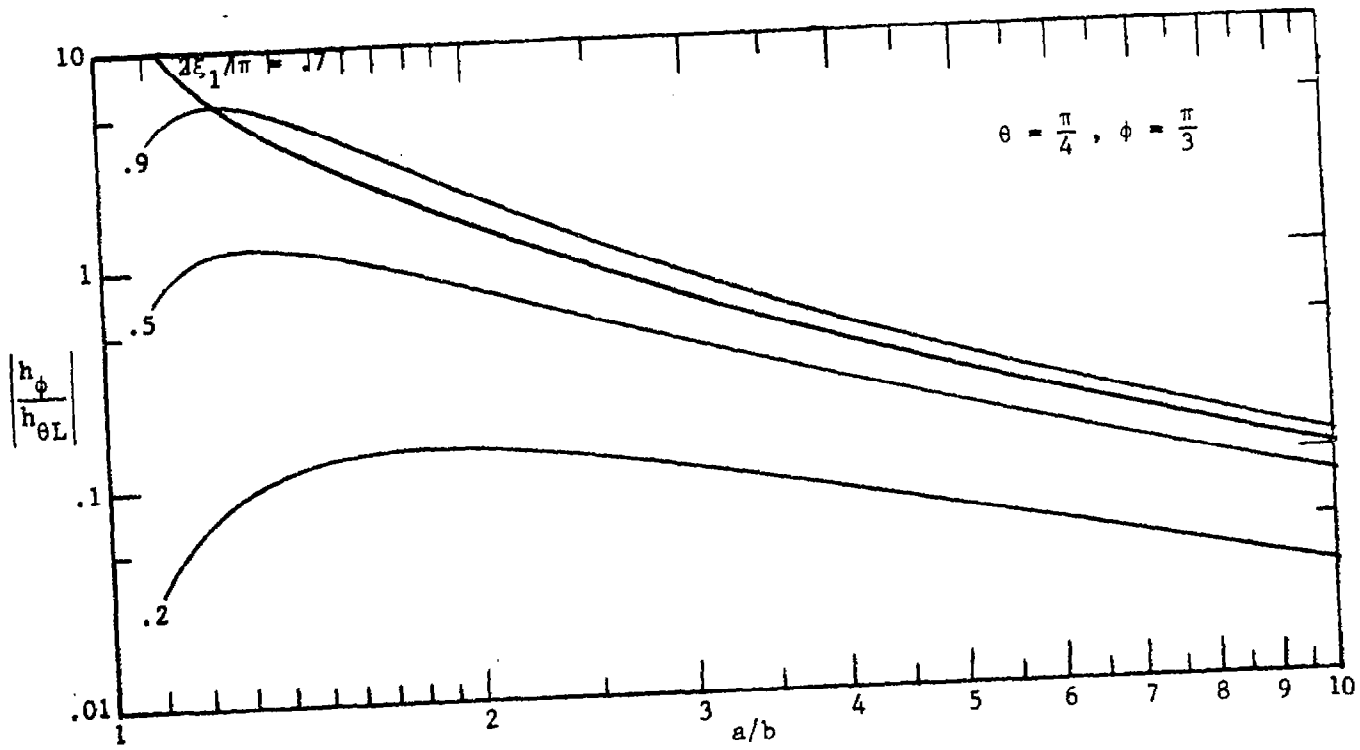


FIGURE 29

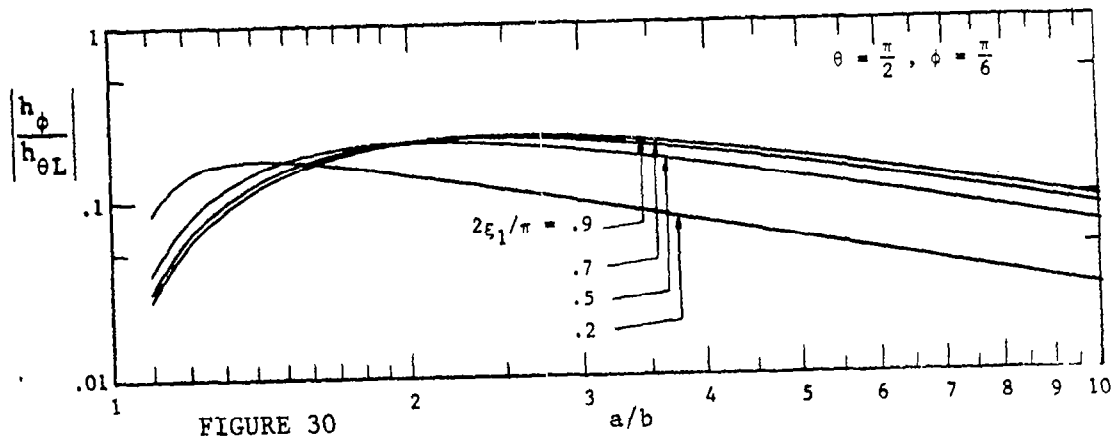


FIGURE 30

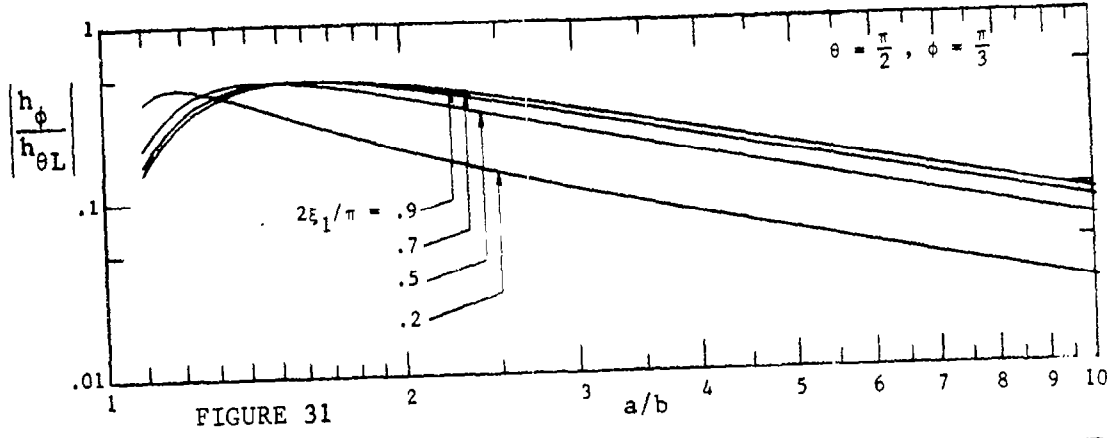


FIGURE 31

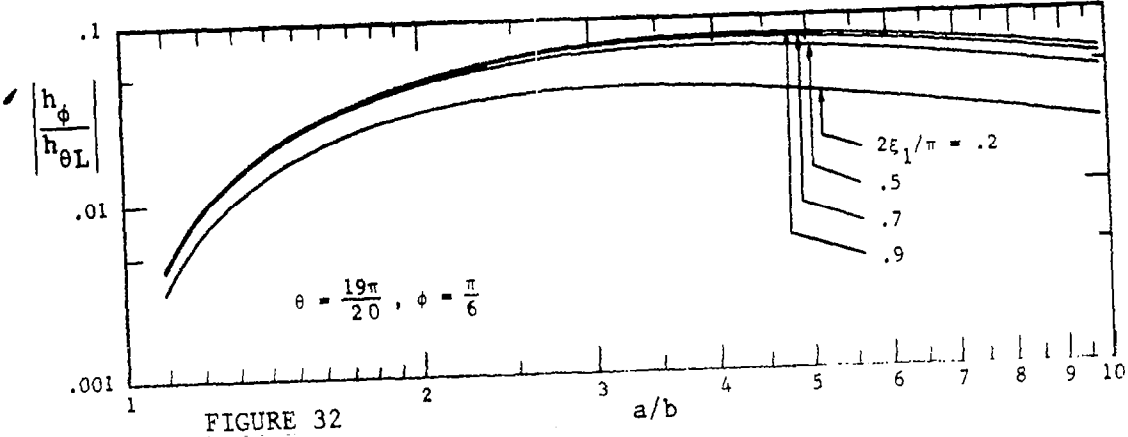


FIGURE 32

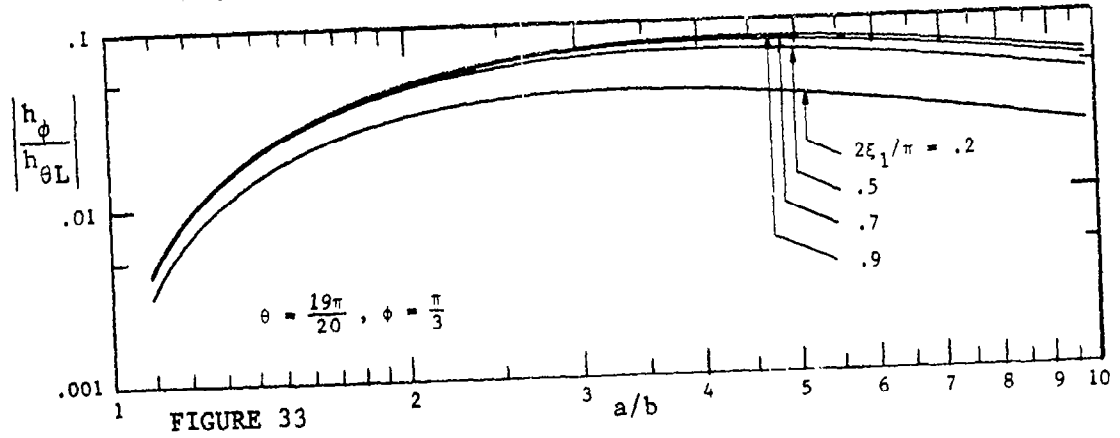


FIGURE 33

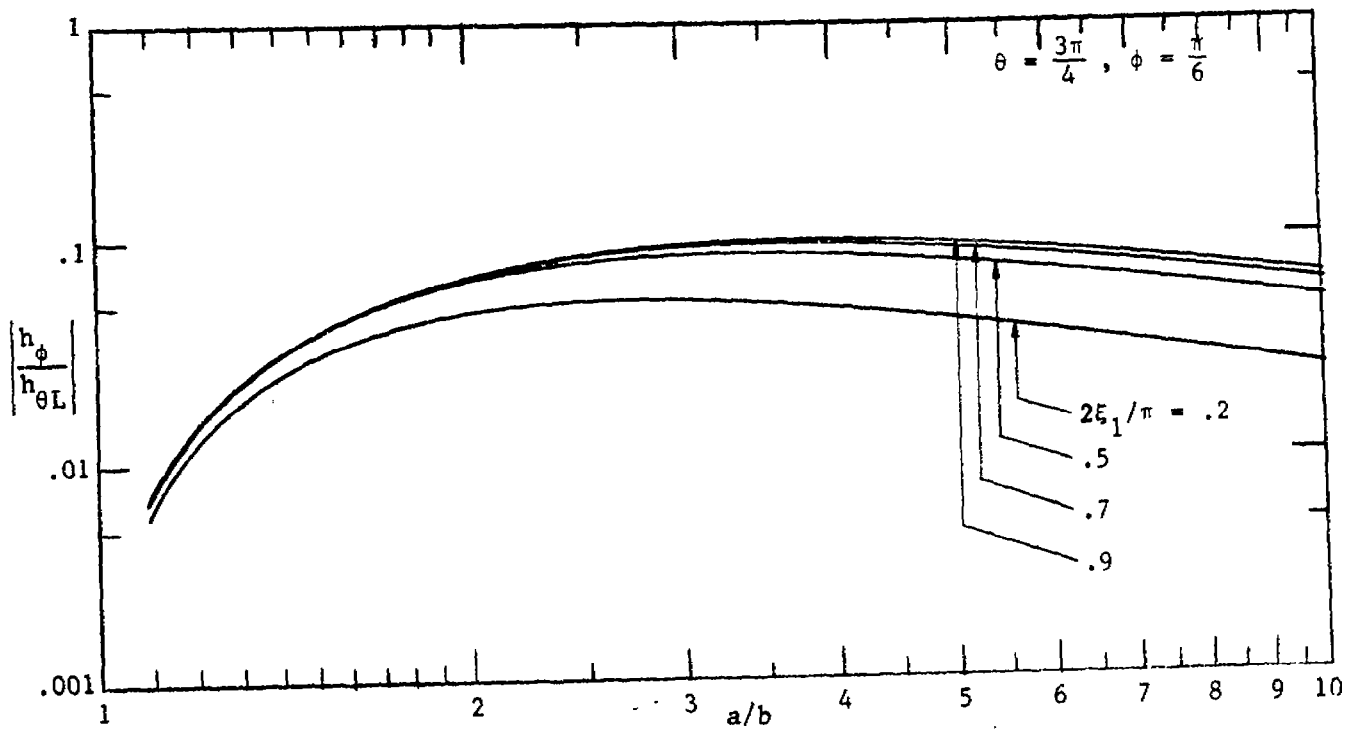


FIGURE 34

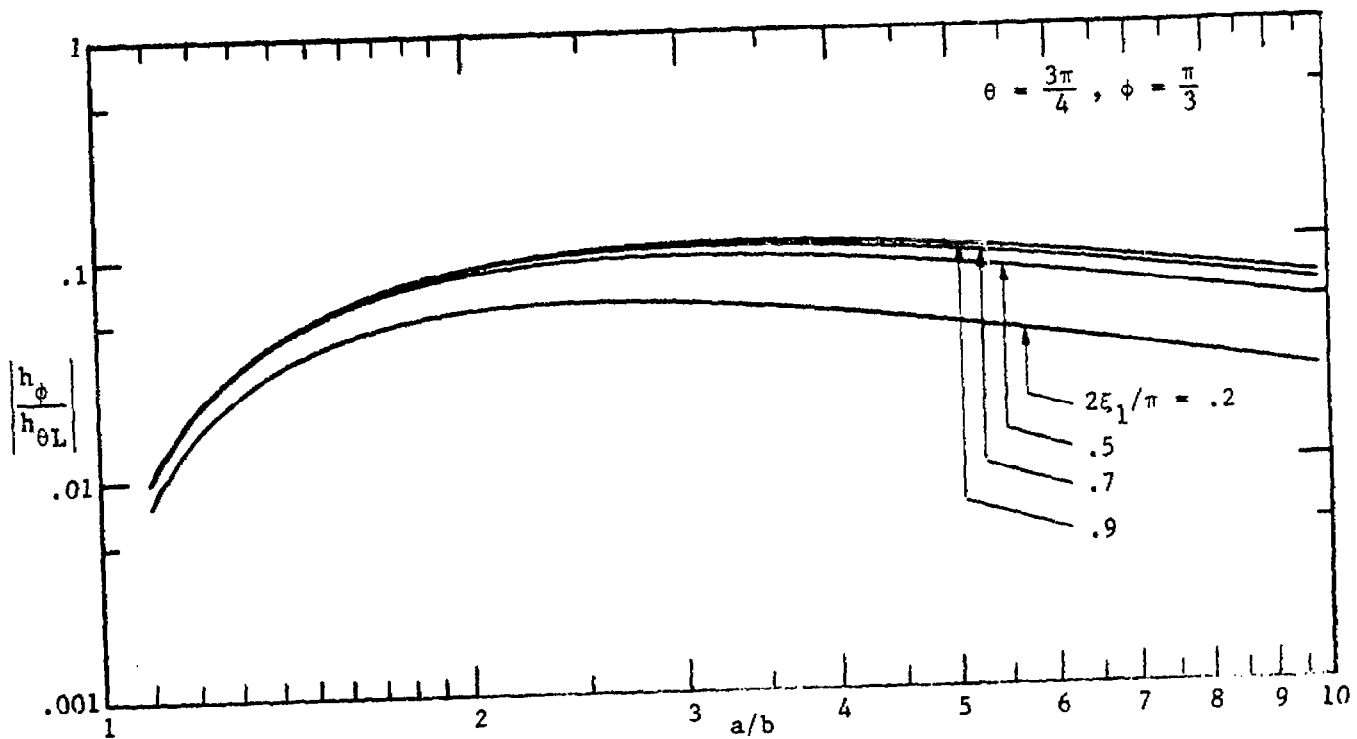


FIGURE 35

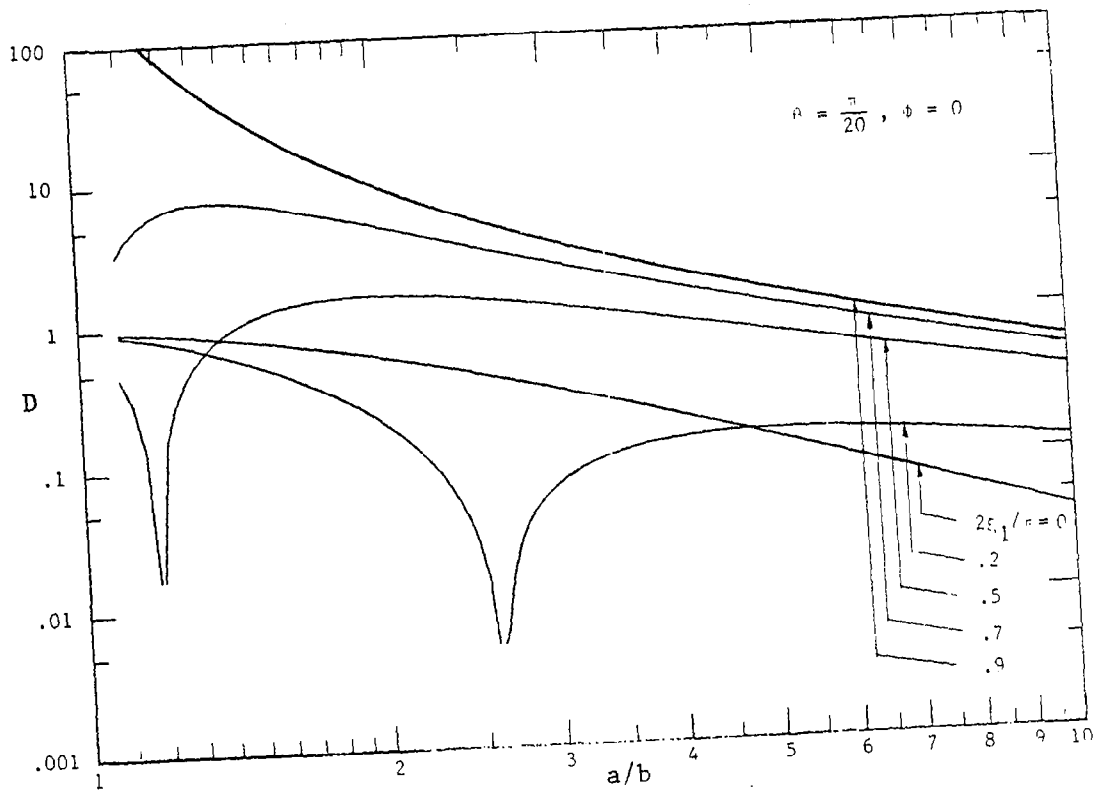


FIGURE 36

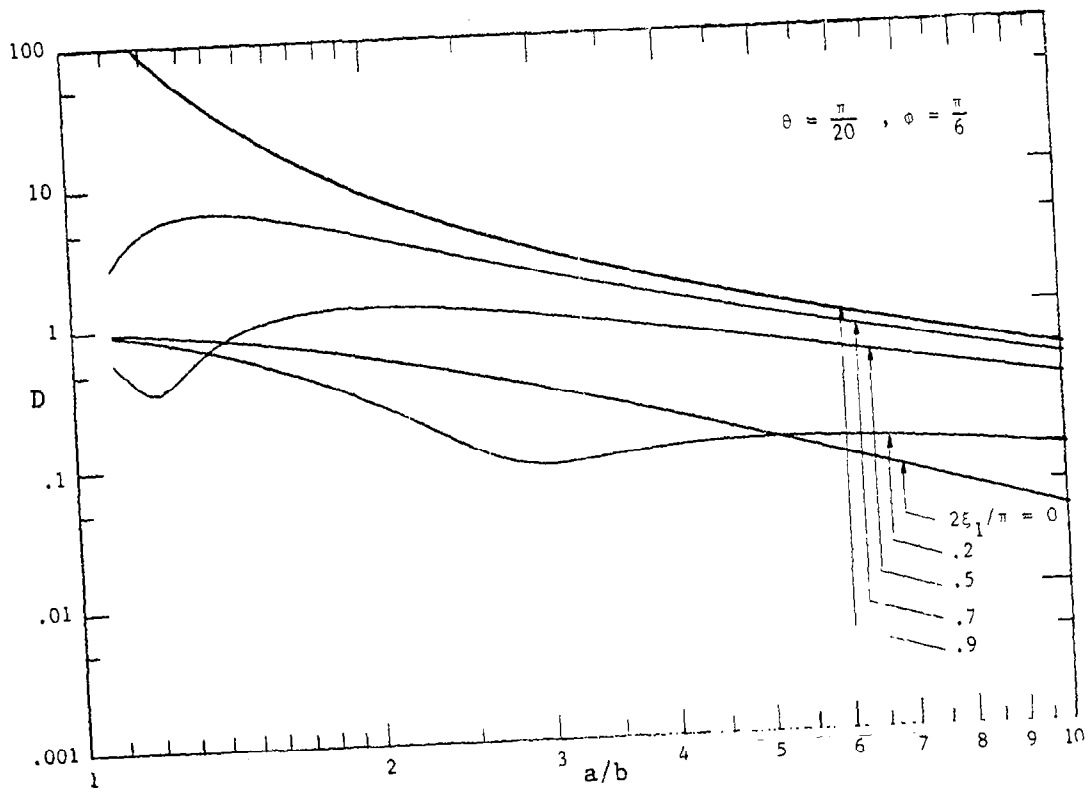


FIGURE 37

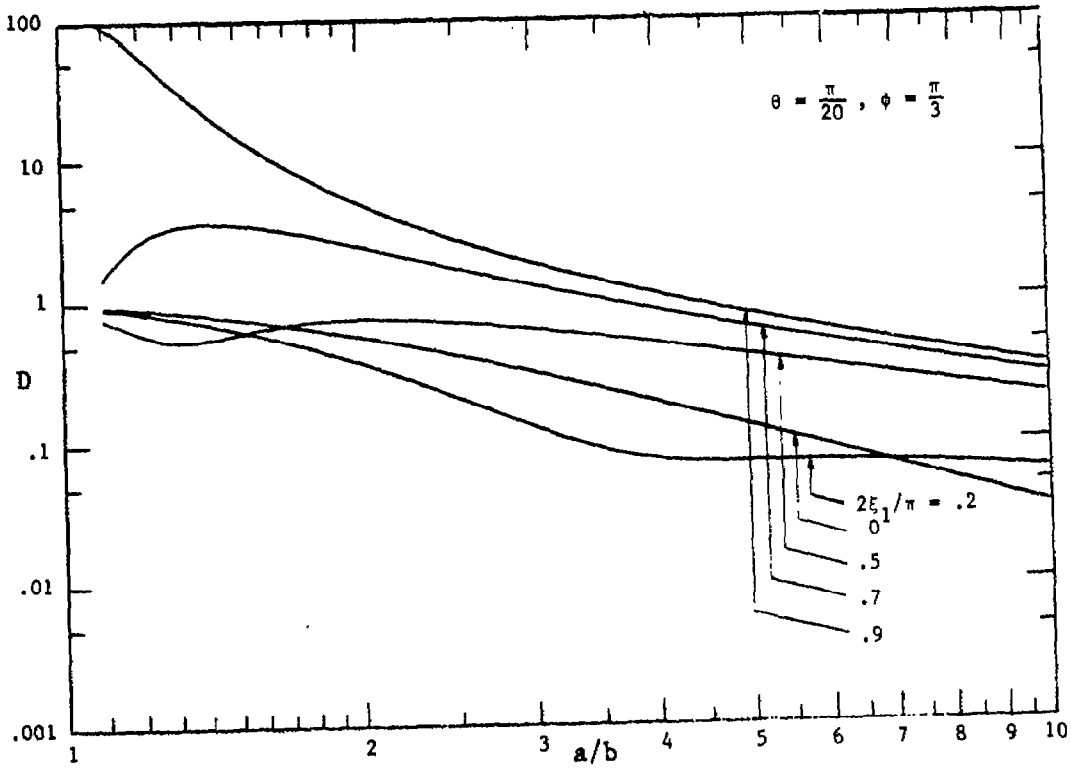


FIGURE 38

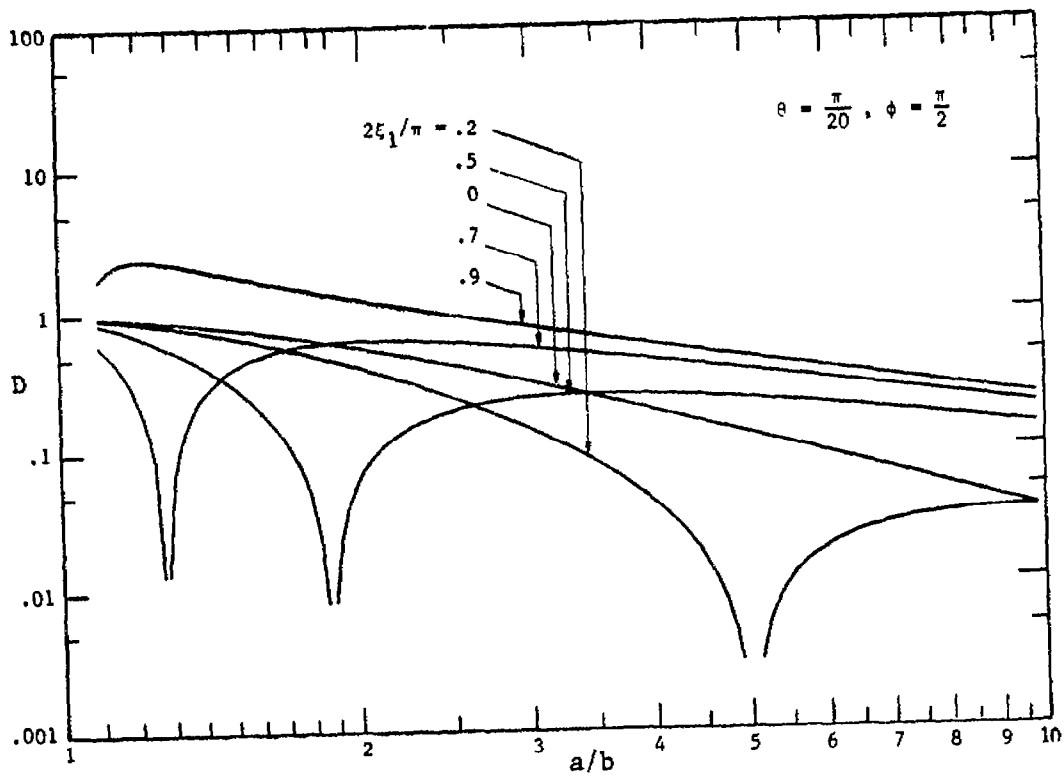


FIGURE 39

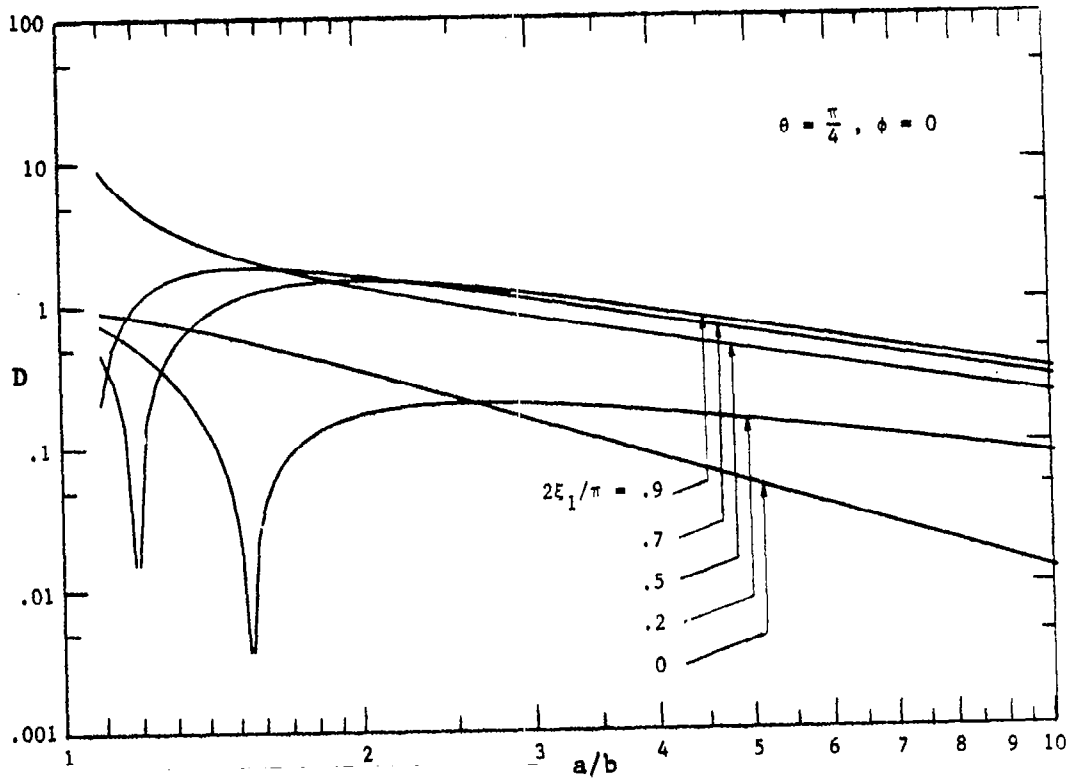


FIGURE 40

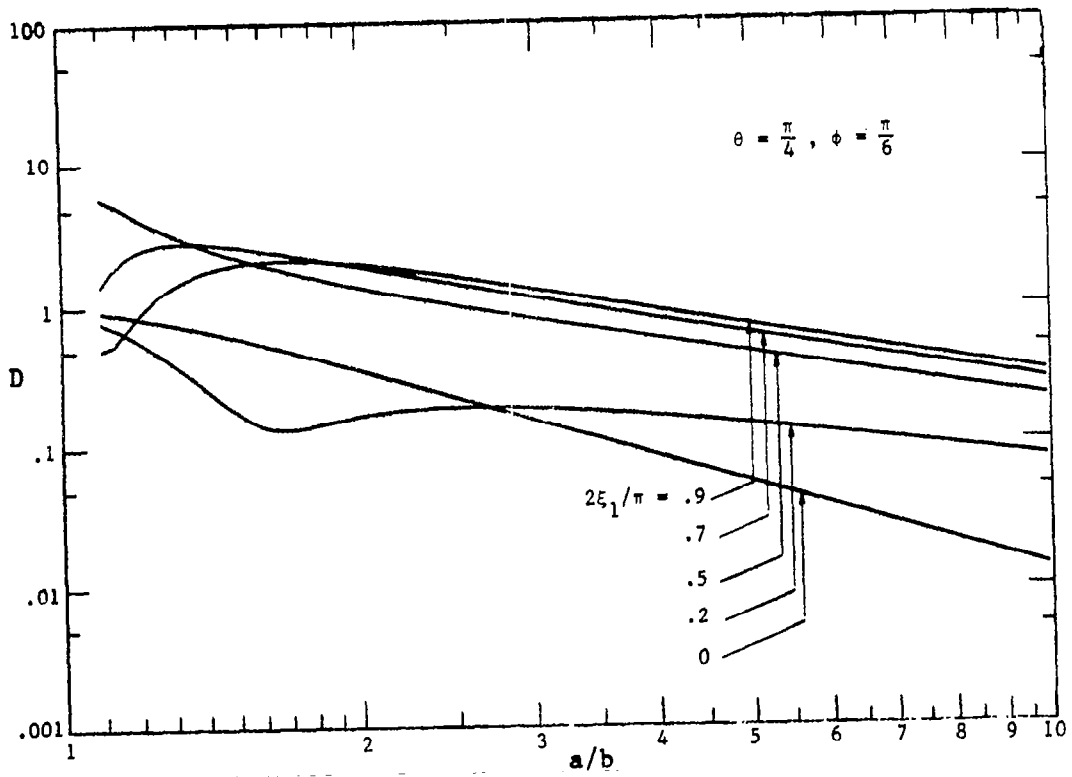


FIGURE 41

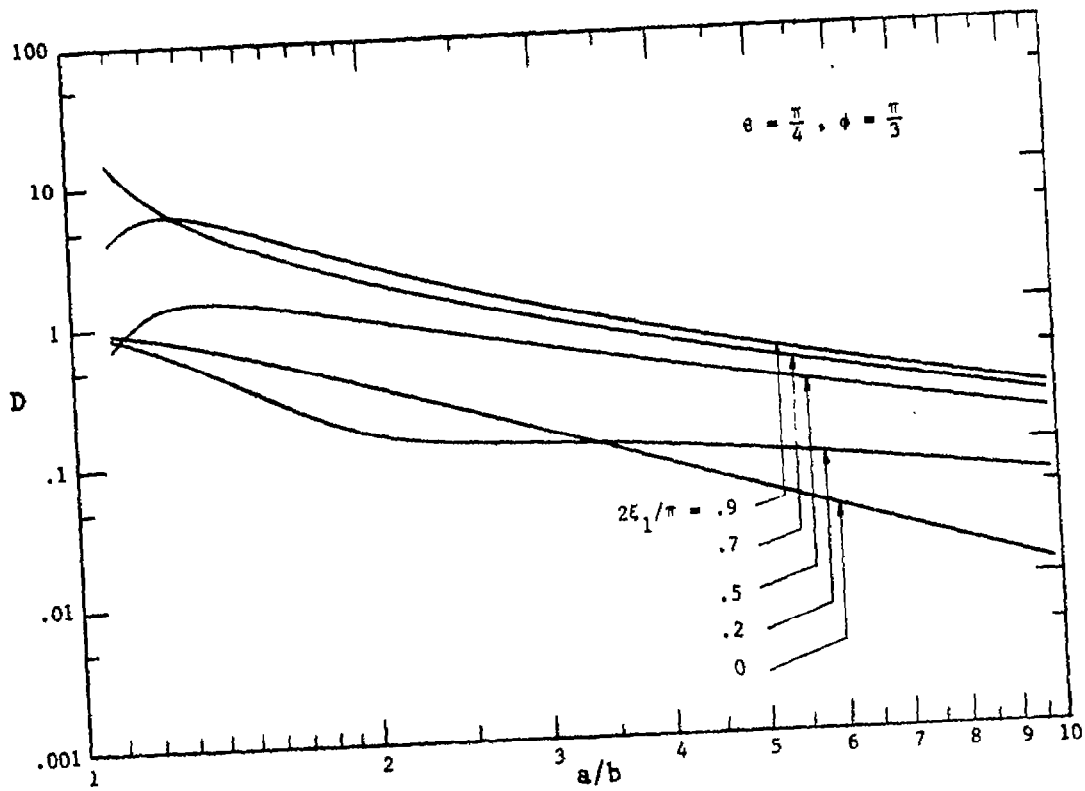


FIGURE 42

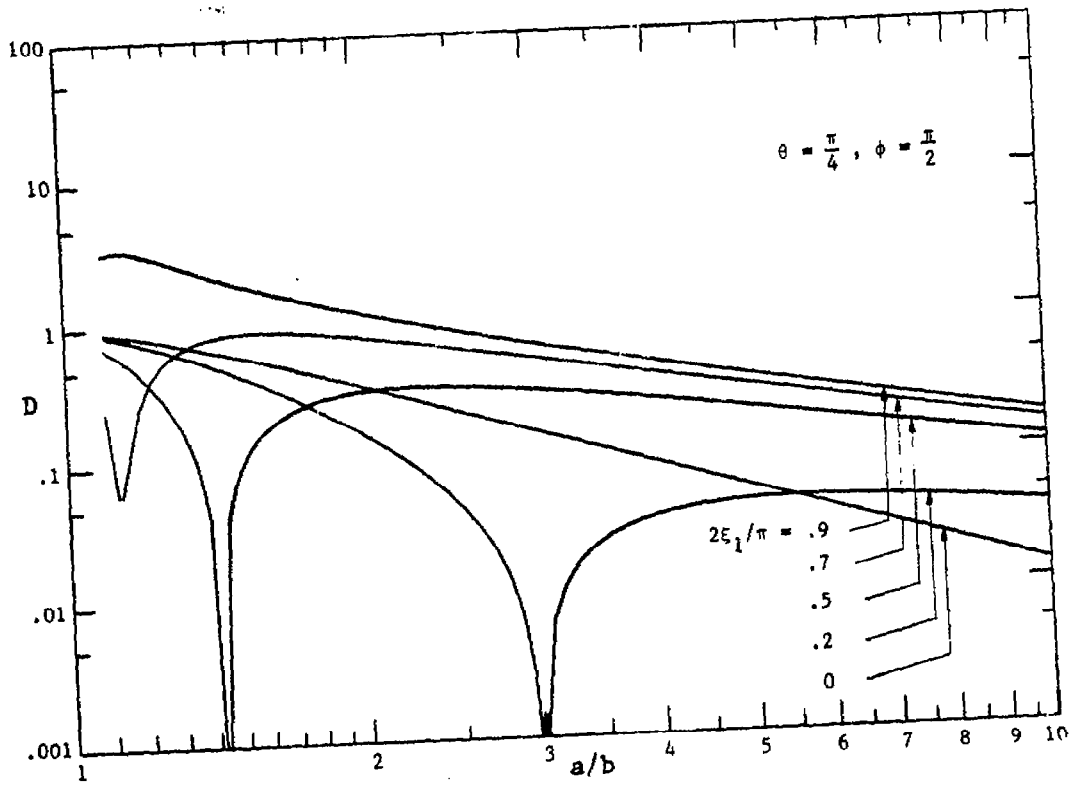


FIGURE 43

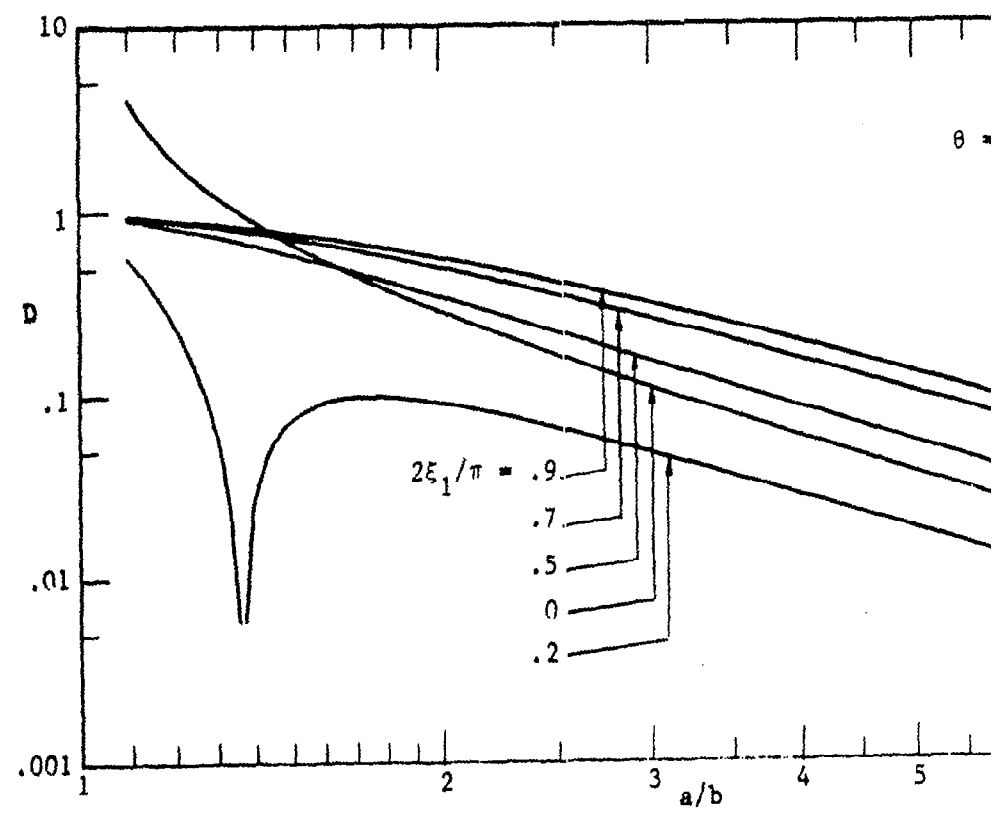
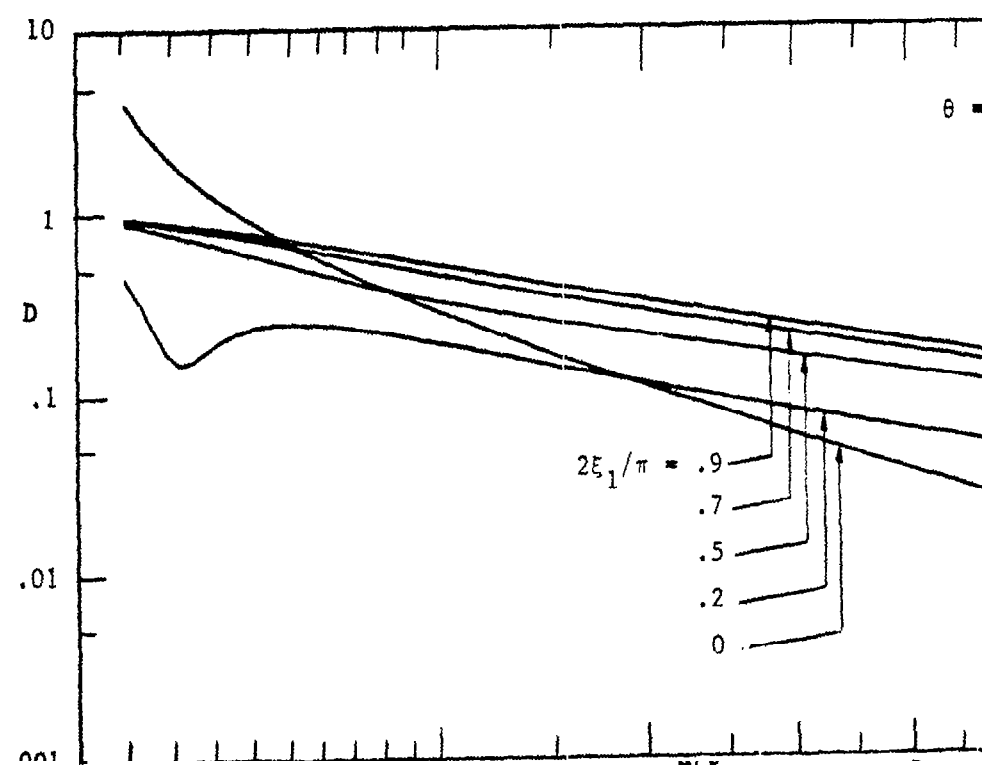


FIGURE 44



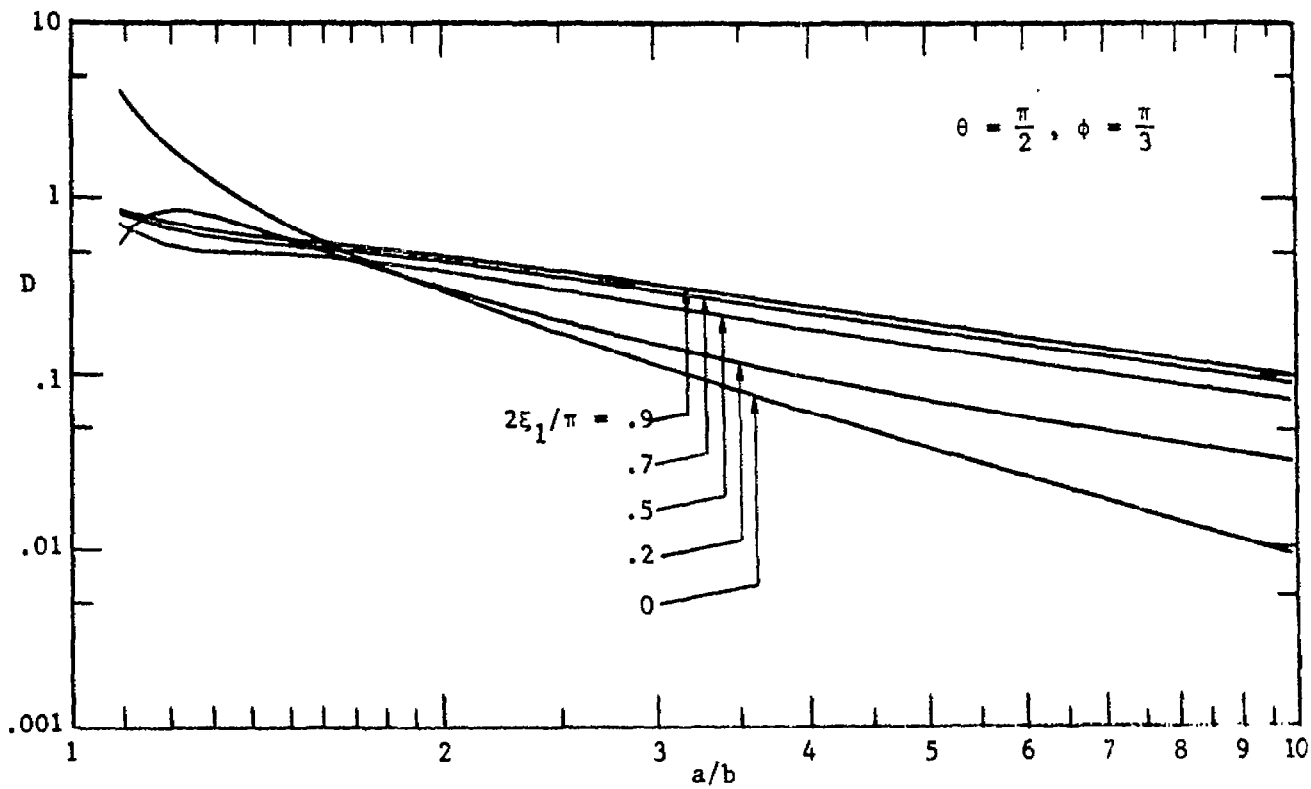


FIGURE 46

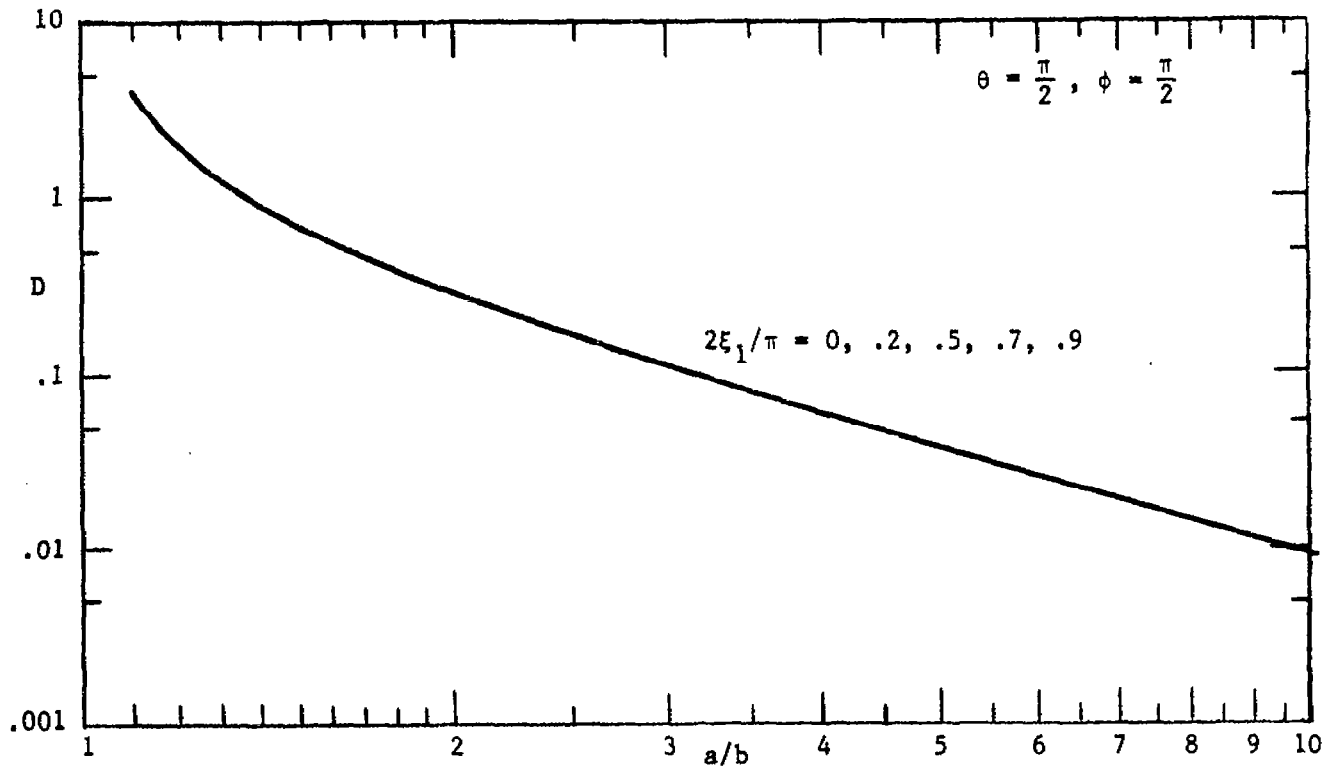


FIGURE 47

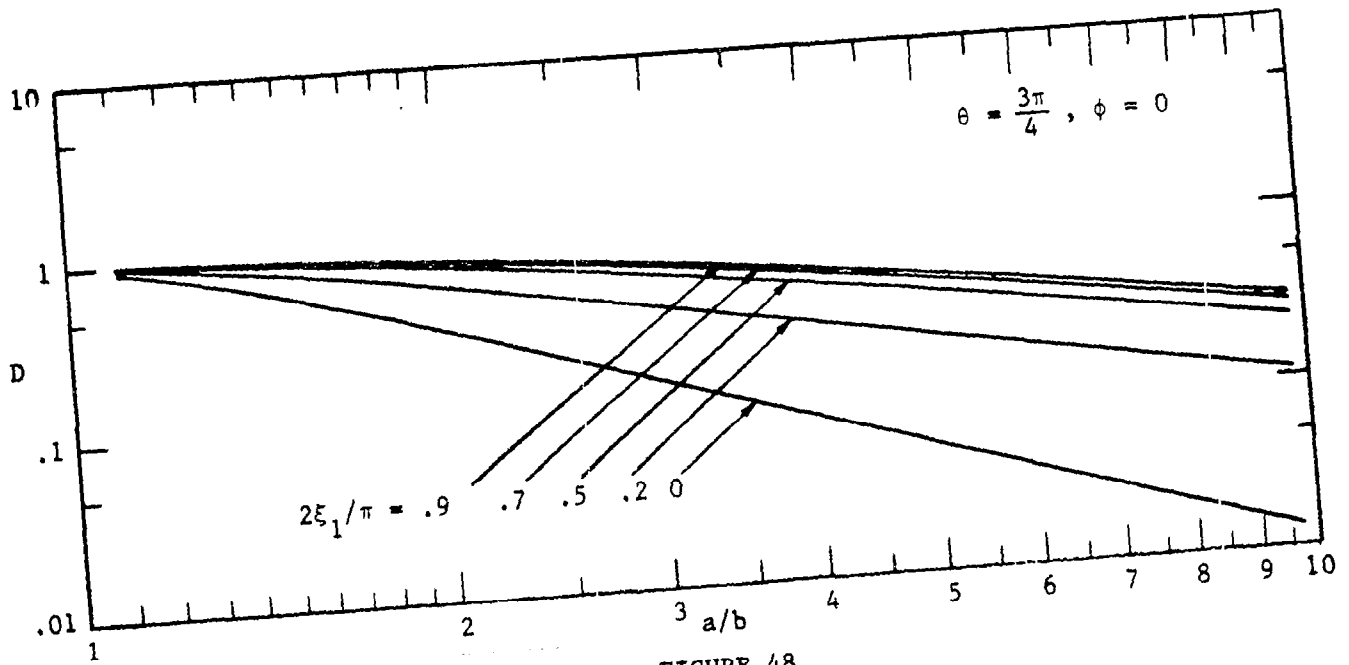


FIGURE 48

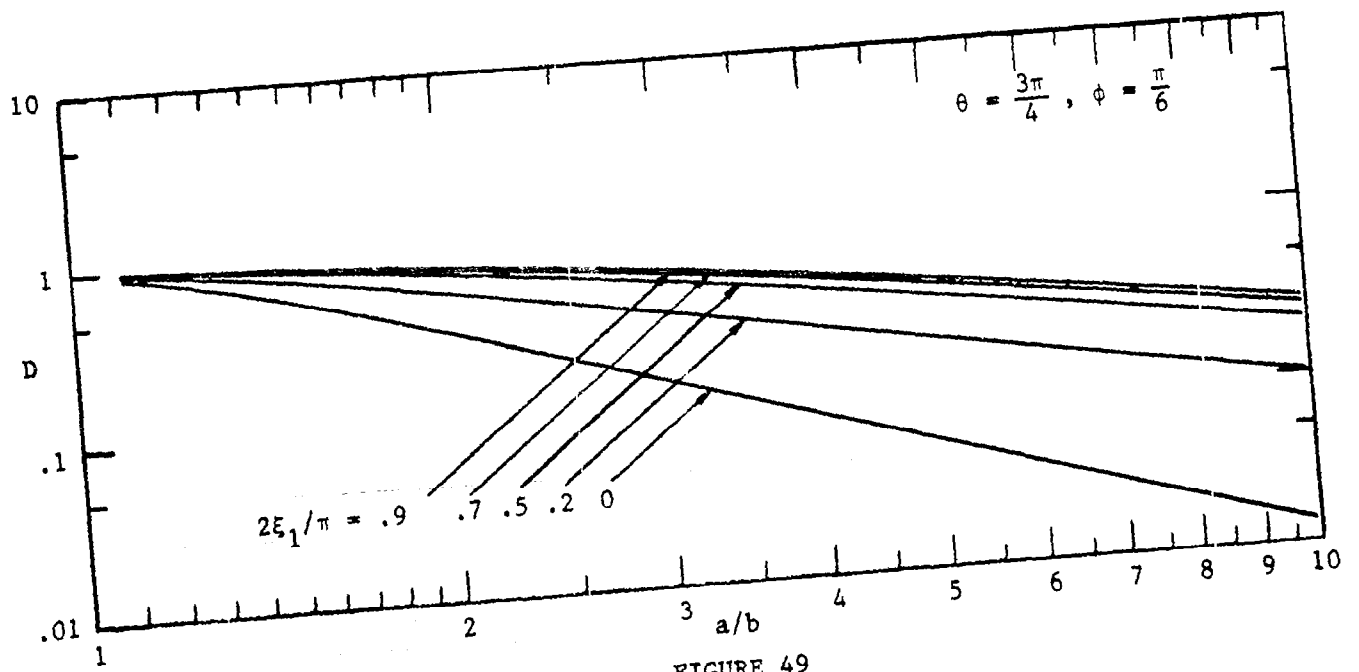


FIGURE 49

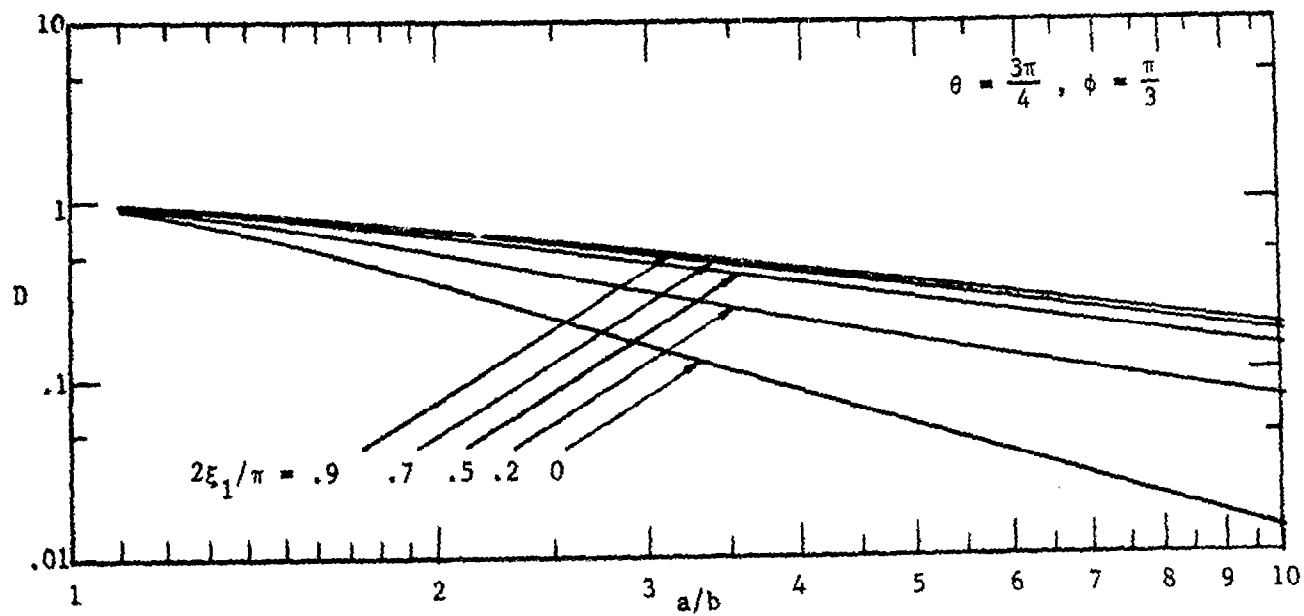


FIGURE 50

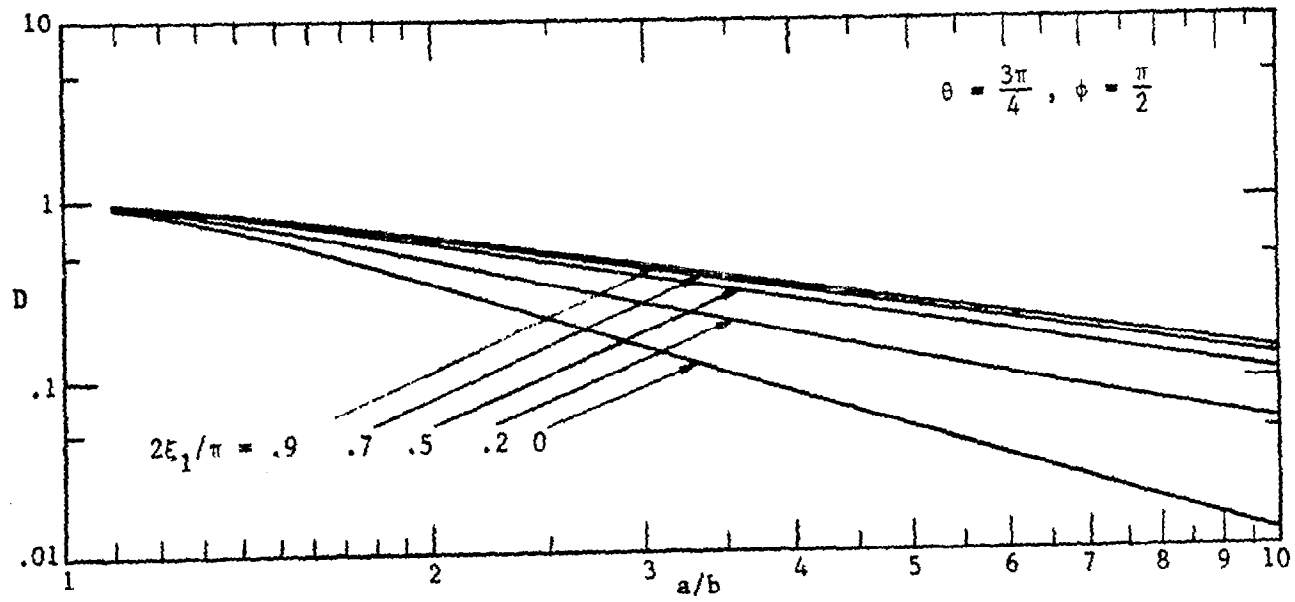


FIGURE 51

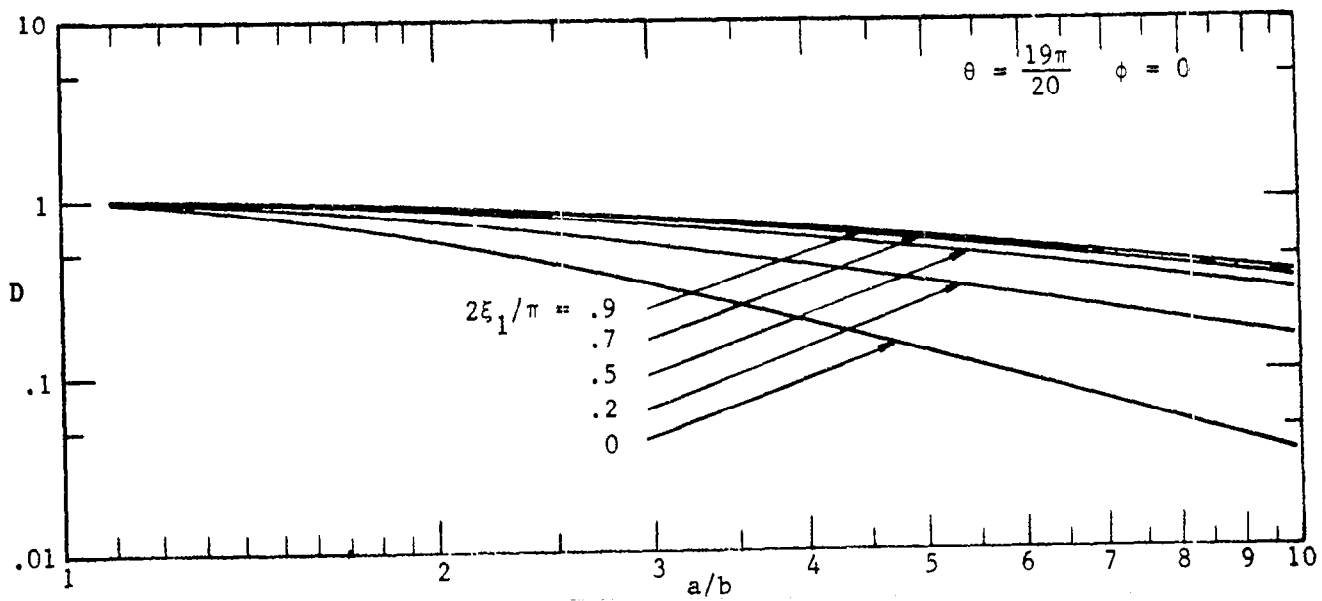


FIGURE 52

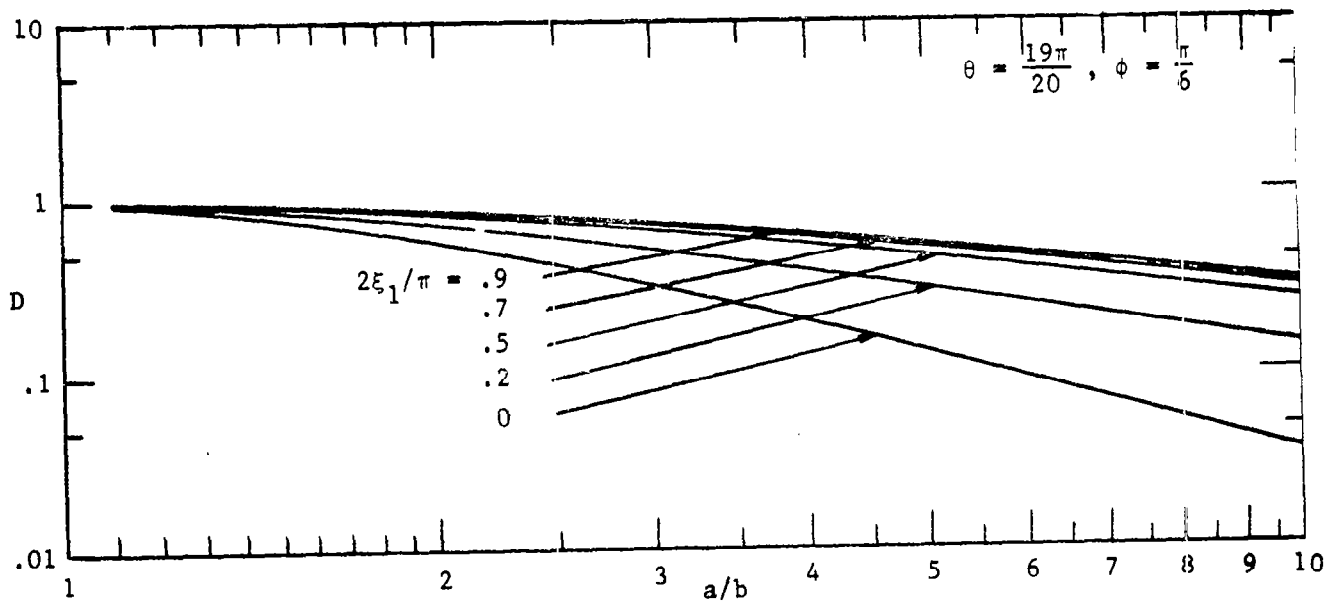


FIGURE 53

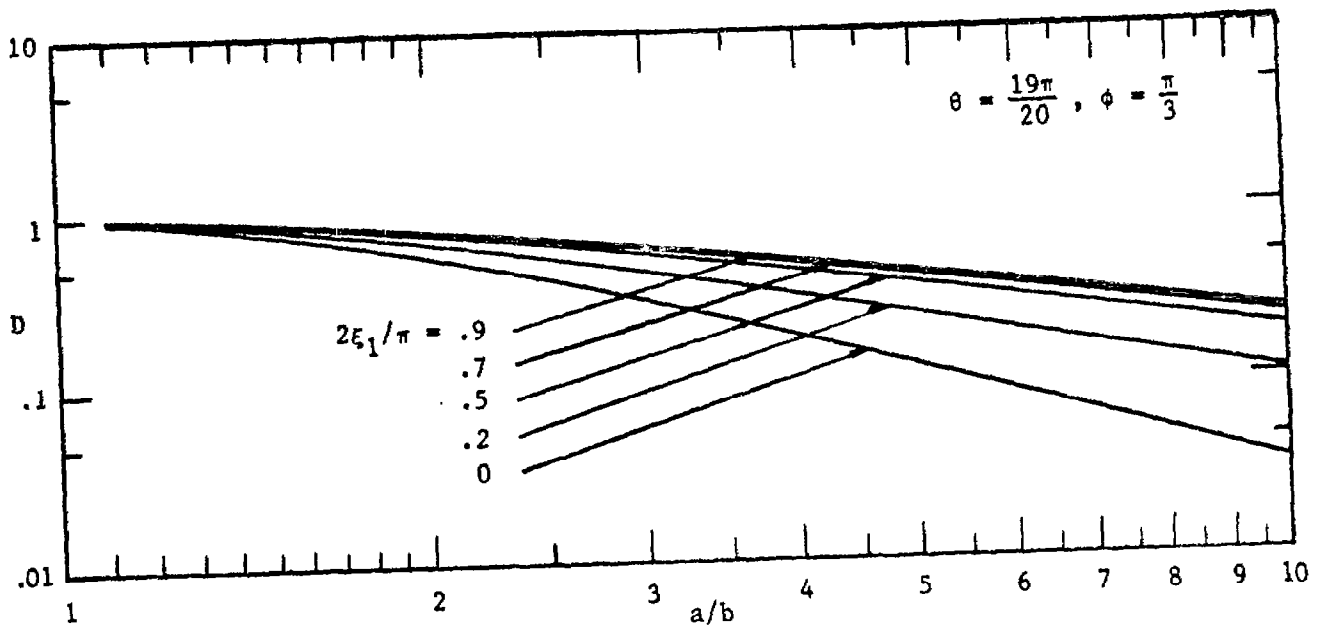


FIGURE 54

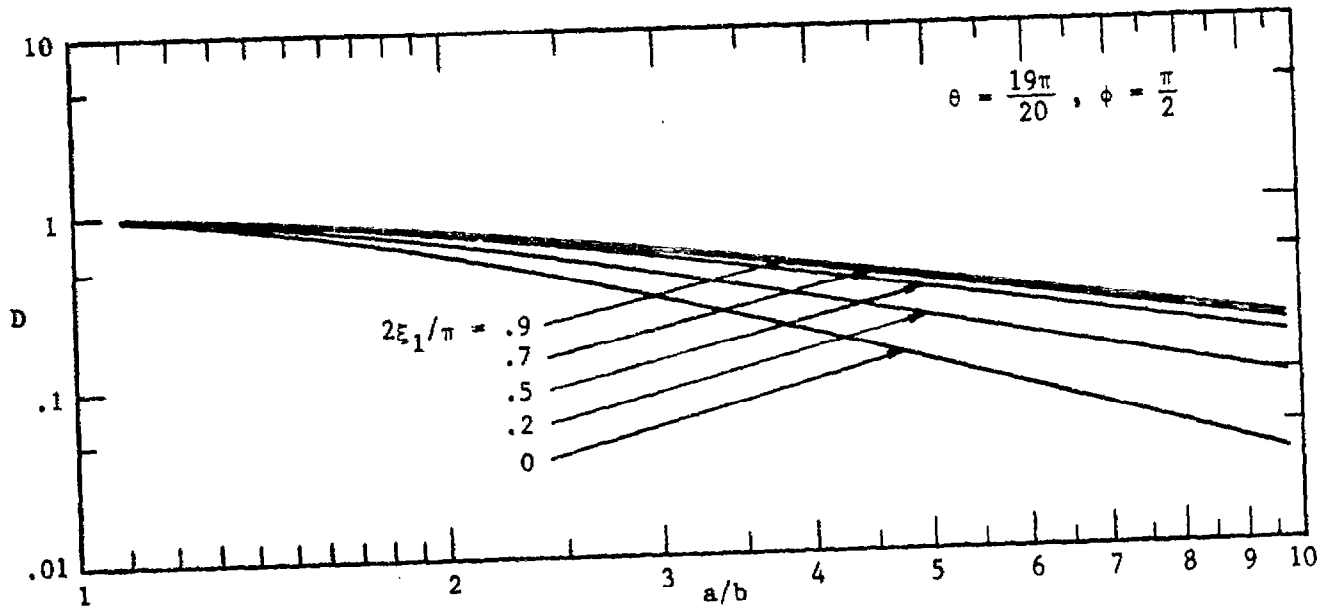


FIGURE 55

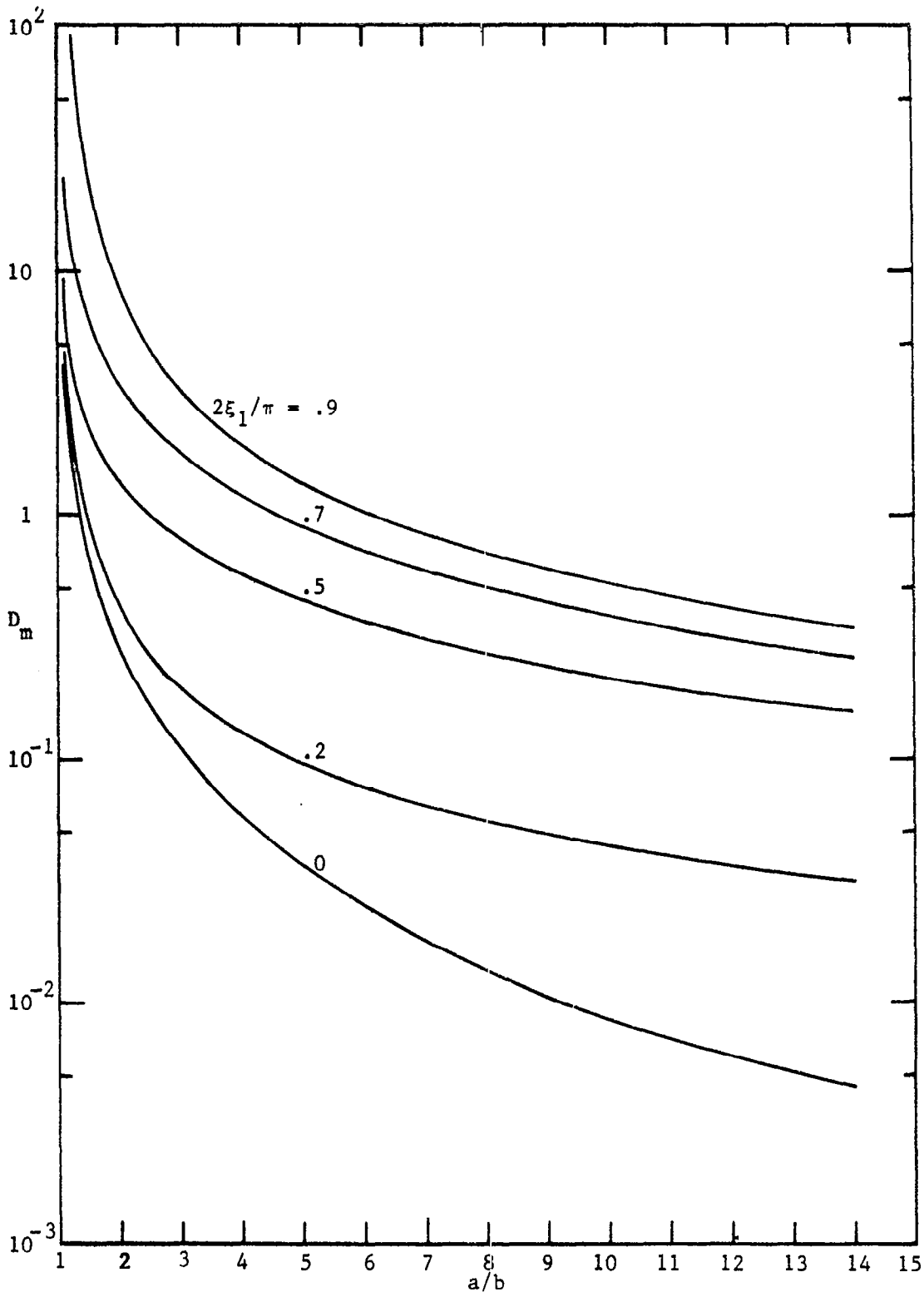


FIGURE 56. D_m is defined as the ratio $(\max D_v)/|h_{\theta L}|$, where the magnetic field deviation D_v has been maximized over the surface of the hemisphere and $|h_{\theta L}|$ has been evaluated at the point where the maximum occurs.

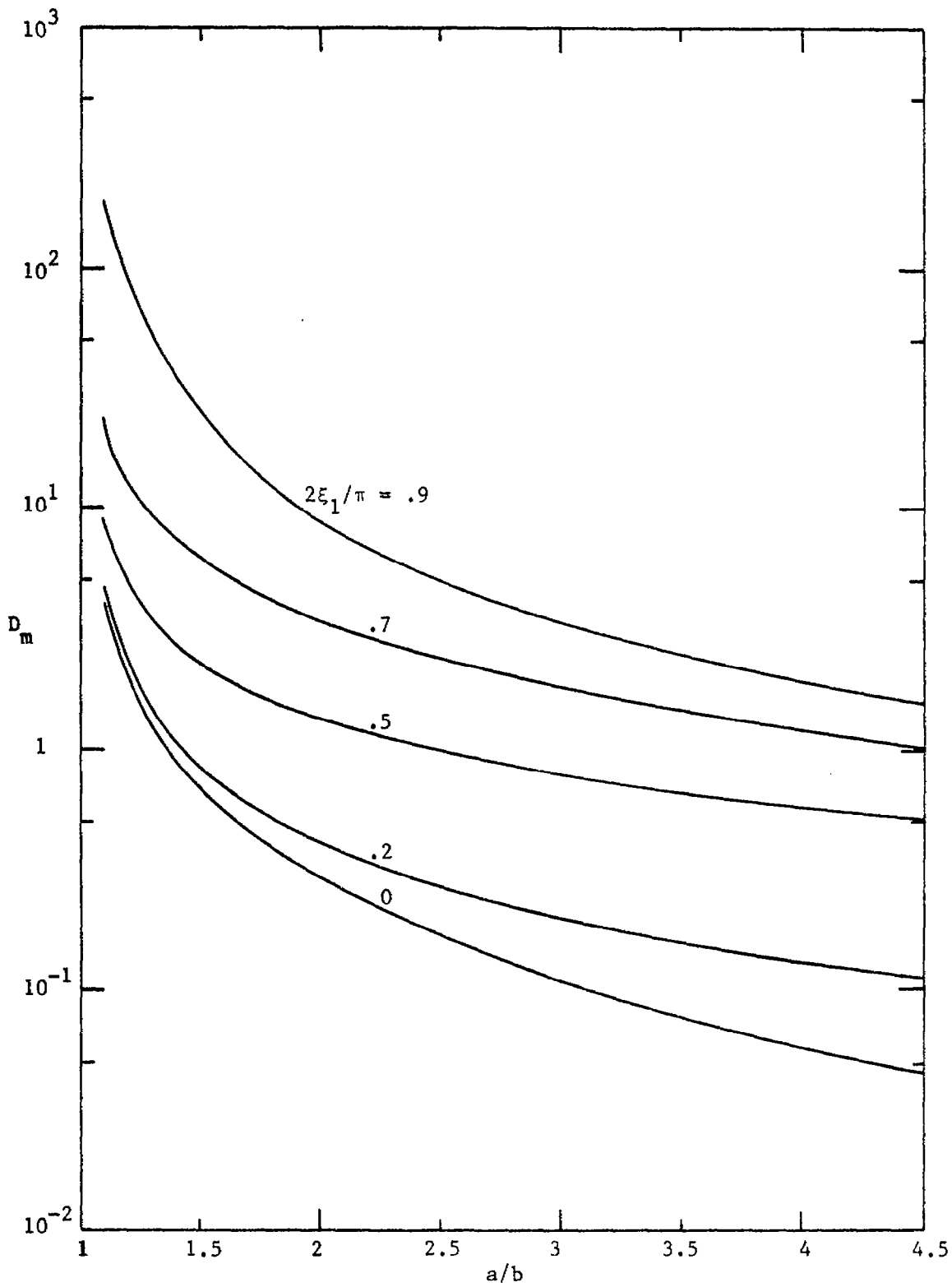


Figure 57. D_m is defined as the ratio $(\max D_v)/|h_{\theta L}|$, where the magnetic field deviation D_v has been maximized over the surface of the hemisphere and $|h_{\theta L}|$ has been evaluated at the point where the maximum occurs.

Acknowledgement

We thank Mr. R. W. Sassman whose computer programming was indispensable and we also thank Dr. C. E. Baum for his helpful comments.

References

1. Capt. Carl E. Baum, Sensor and Simulation Note No. 94, Some Considerations Concerning a Simulator with the Geometry of a Half Toroid Joined to a Ground of Water Surface, November 1969.
2. Capt. Carl E. Baum, Sensor and Simulation Note No. 112, Low-Frequency Magnetic Field Distribution for a Half Toroid Joined to the Surface of a Medium with Infinite Conductivity, July 1970.